Changes in the impacts of ship emissions on $PM_{2.5}$ and its components in China under the staged fuel oil policies

Guangyuan Yu[1,2], Yan Zhang[1,3,4*], Qian Wang[2], Zimin Han[1], Shenglan Jiang[1], Fan Yang[5], Xin Yang[6], and Cheng Huang[2*]

[1]Shanghai Key Laboratory of Atmospheric Particle Pollution and Prevention (LAP[3]), National Observations and Research Station for Wetland Ecosystems of the Yangtze Estuary, Department of Environmental Science and Engineering, Fudan University, Shanghai 200438, China

[2]Shanghai Environmental Monitoring Center (SEMC), Shanghai 200235, China

[3]Shanghai Institute of Eco Chongming (SIEC), Shanghai 200062, China

[4]MOE laboratory for National Development and Intelligent Governance, Shanghai institute for energy and carbon neutrality strategy, IRDR ICoE on Risk Interconnectivity and Governance on Weather/Climate Extremes Impact and Public Health, Fudan University, Shanghai 200433, China

[5]Pudong New Area Environmental Monitoring Station, Shanghai 200135, China

[6]Shenzhen Key Laboratory of Precision Measurement and Early Warning Technology for Urban Environmental Health Risks, School of Environmental Science and Engineering, Southern University of Science and Technology, Shenzhen 518055, China

Correspondence to: Yan Zhang (yan_zhang@fudan.edu.cn) and Cheng Huang (huangc@saes.sh.cn)

Abstract. The issue of air pollution caused by ship emissions is becoming prominent with the increasing global shipping activities. China has carried out ~~staged~~ fuel oil policies by three stages in the past few years to meet the requirements of the global low sulfur regulation by the International Marine Organization ~~(IMO), called the IMO Regulation~~. However, the impacts of ~~ship emissions~~staged policies on air quality in China ~~after 2020~~ are not sufficiently understood. This study firstly updated the ship emission inventory including $PM_{2.5}$ components based on field and on-board measurements under the staged fuel oil policies. Then, the impacts of ship emissions on $PM_{2.5}$ as well as its gas precursors and primary and secondary components in China from 2017 to 2021 ~~have been~~were revealed by using the Weather Research and Forecasting (WRF) model and the Community Multi-scale Air Quality (CMAQ) model. In the model domain, the 99th percentile of the~~We found that~~ shipping-related $PM_{2.5}$ concentrations was reduced by 19.5% and then by 35.6% due to the policy shifts-. ~~ship~~ Ship emissions increased the $PM_{2.5}$ concentrations up to 3.8 μg m^{-3} in 2017 and 2.6 μg m^{-3} in 2021 ~~along China's coastal area~~. The areas with high concentration levels widely distributed over ~~the~~ offshore waters in 2017, and shrunk to some parts of China's coast in 2021. ~~The seasonal patterns of the shipping related $PM_{2.5}$ concentration differed by region mainly due to the seasonality of secondary aerosol formation.~~ The

contributions of ship emissions to the $PM_{2.5}$ concentrations over China's main port cities ranged from 3.0% to 17.4% in 2017 and 2.5% to 10.3% in 2021. In these cities, the change rates of the concentrations of $PM_{2.5}$, SO_4^{2-}, NO_3^-, NH_4^+, carbonaceous aerosols, V, and Ni related to ship emissions from 2017 to 2021 were -32.7%, -74.0%, +11.0%, -27.5%, -76.9%, -90.3%, and -38.4%, respectively. NO_3^- constituted 54.6% of the shipping-related $PM_{2.5}$ in 2021. ~~The sea-land breeze circulation played an important role in the diurnal patterns of the concentrations of primary particulate matter from shipping in most seaports, while a minor role was found in Shanghai and Guangzhou where both inland and marine ship emissions are considerable.~~ Our findings suggest that it is important to consider both transport pathways and secondary aerosol formation mechanisms ~~of secondary aerosols~~ to combat the $PM_{2.5}$ pollution caused by shipping in different regions.

1 Introduction

Shipping is the backbone of global trade and transports more than 80% of global goods. The global shipping activities increased by ~20% in the past decade, and continues to grow at a rate of ~2% per year in the coming years (UNCTAD, 2023). Meanwhile, heavy fuel oil (HFO) is the most widely used type of fuels for marine vessels. The combustion of HFO can release remarkably higher amounts of sulfur oxides (SO_x), particulate matter (PM), and trace elements compared to the combustion of lighter oils (Agrawal et al., 2008a; Moldanová et al., 2013; Zhang et al., 2019b). Due to the increasing shipping activities and the low quality of fuel oils, shipping is becoming an important source of air pollution, especially in coastal areas and ports with dense traffic (Dalsøren et al., 2009; Eyring et al., 2010). It is reported that international vessels emitted 9600 kt (kilotons) SO_x, 17100 kt NO_x (nitrogen oxides), and 1351 kt $PM_{2.5}$ (PM with a diameter of less than 2.5 μm) in 2018 (IMO, 2021). In Europe, the maritime transport sector produced 24% of all NO_x emissions, 24% of all SO_x emissions, and 9% of all $PM_{2.5}$ emissions in 2018, affecting ~40% of Europeans living within 50 km of the sea (EMSA and EEA, 2021). In 2022, China held a national port cargo throughput of 15.68 billion tons, and was home to eight of the top ten ports for cargo throughput and seven of the top ten ports for container throughput worldwide (Ministry of Transport of the People's Republic of China, 2023). Tracking ship emissions and their environmental impacts in China is of great significance.

Exposure to high levels of $PM_{2.5}$ can increase health problems like respiratory and cardiovascular

diseases. The World Health Organization (WHO) Global Air Quality Guidelines 2021 recommend that annual mean concentrations of $PM_{2.5}$ should not exceed 5 μg/m^3 (WHO, 2021). Studies using chemical transport models (CTMs) have been conducted to simulate the impact of ship emissions on $PM_{2.5}$ in the regions with heavy ship traffic. In China, ship emissions increased the annual averaged $PM_{2.5}$ concentrations up to 5.2 μg m^{-3} in 2015, surpassing the limit value supposed by the WHO. In Europe and North America, the increase in $PM_{2.5}$ concentrations due to shipping is generally less than 2 μg m^{-3}; however, its relative contribution is significant, reaching 25%−50% along main shipping routes and 12%−15% in coastal areas (Aksoyoglu et al., 2016; Tang et al., 2020; Fink et al., 2023a; Golbazi and Archer, 2023). Based on observation, the impact of ship emissions on PM can also be calculated by using source apportionment methods like receptor models. In China, our previous studies show that ship emissions contribute 1.96 μg m^{-3} (4.23%) to the ambient $PM_{2.5}$ concentration at port, while 0.4−3.1 μg m^{-3} (1.3%−8.8%) for downtown Shanghai (Zhao et al., 2013; Yu et al., 2021); the fraction of shipping-related particles is 1%−10% in port cites (Liu et al., 2017b; Wang et al., 2019; Zhang et al., 2019a; Zhai et al., 2023). Ship emissions contribute to annual mean concentrations of $PM_{2.5}$ with 1%−14% in European coastal areas and 3%−9% in American coastal areas (Agrawal et al., 2009; Viana et al., 2014; Kotchenruther, 2015; Anastasopolos et al., 2021).

Shipping-related PM is comprised of primary particles and secondary products. Ships primarily emit organic carbon (OC), elemental carbon (EC), sulfate, metallic elements, etc., among which OC and sulfate are the main components of primary PM from ships burning HFO (Agrawal et al., 2008b; Lack et al., 2009; Agrawal et al., 2010; Huang et al., 2018a; Yang et al., 2022; Karjalainen et al., 2022). Vanadium (V), nickel (Ni), and the V/Ni ratio are the mostly used tracers of ship emissions (Agrawal et al., 2009; Moldanová et al., 2009; Celo et al., 2015; Corbin et al., 2018; Yu et al., 2021). Calculating the emissions, the concentrations, and the deposition fluxes of V and Ni from shipping can help better understanding their geochemical cycles. In comparison, sulfate, nitrate, and ammonium (SNA) dominate the shipping-related PM with its proportion even exceeding 90% based on modeling research (Lv et al., 2018; Jonson et al., 2020; Fink et al., 2023a; Jang et al., 2023).

Studies have demonstrated that using desulfurized fuel oils can significantly reduce the emissions of various air pollutants such as SO_x, PM, OC, heavy metals, and polycyclic aromatic hydrocarbons (PAHs) (Tao et al., 2013; Zetterdahl et al., 2016; Kotchenruther, 2017; Spada et al., 2018; Huang et al., 2018a). To combat the air pollution caused by ship emissions, four Emission Control Areas (ECAs) have been

established in Europe and North America since 2011. The sulfur limits for fuel in the ECAs was restricted to 0.10% m/m after 1 January 2015. Besides, the Tier III that regulates the NO_x emission factor no more than 3.4 g/kWh entered into force on 1 January 2016 in the ECAs of North America and on 1 January 2021 in the ECA areas of Europe. However, the regulations in China are significantly lagging behind those in North America and Europe. The global fuel sulfur limit of 0.50% (reduced from 3.50%) has been mandated by the International Maritime Organization (IMO) since 1 January 2020, which is called the IMO Regulation. Before 2017, marine vessels in China region generally used HFO with a sulfur content of ~2.7%. To meet the IMO Regulation, the Ministry of Transport of China enacted staged control policies from 2017 to 2020. Ships berthing at the ports in the China's Domestic Control Areas (DECAs) were required to use fuel with a sulfur content no more than 0.50% (low sulfur fuel oil, LSFO hereafter) after 1 January 2017, which is called the DECA 1.0 period. All ships within 12 nm (nautical miles) from the baseline of the territorial sea~~coastline~~ must use LSFO after 1 January 2019, which is referred to as the DECA 2.0 period (Liu et al., 2018a; Wang et al., 2021). The inland emission control areas covering the Yangtze River, the Xijiang River, and the Pearl River went into effect after 1 January 2019 where coastal vessels were required to combust LSFO; both coastal and international vessels must use fuel with a sulfur limit of 0.10% called ultra-low sulfur fuel oil (ULSFO) after 1 January 2020. ~~The rapid transition of China's control measures is to meet the global fuel sulfur limit of 0.50% (reduced from 3.50%) from 1 January 2020 mandated by the IMO (the IMO Regulation).~~ The staged regulations for fuel sulfur content are summarized in Table S1. For the NO_x emission control, newly built ships in China follow the IMO Tier II standard from 2011 that regulates the NO_x emission factor no more than 14.4 g/kWh~~from 2011.~~ (Yi et al., 2025; Wang et al., 2025; Luo et al., 2024; Song et al., 2022; Jang et al., 2023)

Latest published studies have reported the effects of the implementation of the IMO Regulation in global and regional scales. In 2020 relative to 2019, both the sulfur dioxide (SO_2) and $PM_{2.5}$ emissions from shipping were reduced by ~80% in a global scale (Yi et al., 2025; Wang et al., 2025). In China, 调 the shipping-related $PM_{2.5}$ concentrations decreased but mortality increased in port cities from 2016 to 2020 (Luo et al., 2024). In South Korea, the SO_2 and NH_4^+ concentrations as well as the contributions of shipping to sulfate and OC decreased after 2020 (Song et al., 2022; Jang et al., 2023). However, there are few studies on the impacts of ship emissions on multiple atmospheric pollutants after the implementation of the IMO Regulation based on actual shipping activity data and CTMs~~The staged sulfur regulations are expected to effectively alleviate the air pollution from shipping in China . However, there are very few~~

~~studies on the impacts of ship emissions on air quality after the implementation of the IMO Regulation based on actual shipping activity data and CTMs~~ (Zhai et al., 2023; Feng et al., 2023~~(Luo et al., 2024)~~). ~~For instance, t~~The simulation years of ~~the~~ some ~~recently published~~ studies published in the past two years from China, Europe, and North America are ~~generally~~ before the IMO Regulation (Fink et al., 2023b; Fu et al., 2023; Golbazi and Archer, 2023). Yet there is little knowledge on the changes in the impacts of ship emissions on air quality under staged fuel oil policies in China since 2017 as well as~~There is relatively little research on simulating~~ the changes in the s~~s~~pecific composition of shipping-related PM. The impacts of meteorology and chemical mechanisms on the $PM_{2.5}$ pollution caused by shipping in China are not fully understood. In addition, it has been observed that the concentrations of V and Ni from shipping decreased significantly and stepwise in China's largest port city from 2017 to 2020 in our previous study. The latest emission inventories of V and Ni from shipping are still not earlier than 2017, and need updating until after 2020 (Zhao et al., 2021; Jiang et al., 2024).

In this study, we updated the ship emission inventory based on the data from the Automatic Identification System (AIS), and simulated the impacts on $PM_{2.5}$ in China as well as its gas precursors (SO_2 and NO_2) and components from 2017 to 2021 by using the Weather Research and Forecasting (WRF) model and the Community Multi-scale Air Quality (CMAQ) model. The emissions of V and Ni from shipping were constrained by the field observational data from our previous study and the results of on-board emission measurements. Based on the simulation results, the spatiotemporal patterns of shipping-related $PM_{2.5}$ as well as trace elements (V and Ni), secondary inorganic aerosols, and organic aerosols were obtained. Meanwhile, the interannual and seasonal variations of the impacts were investigated. Then, we focused on the changes in the impacts due to the IMO Regulation at the port city level. Besides, the roles of the meteorological factors in affecting the seasonal and diurnal patterns of primary PM from shipping over the port cities were discussed.

2 Methods

2.1 Setup of the WRF/CMAQ

We utilized the CMAQ version 5.4 to simulate the pollutant concentrations, and the WRF version 4.1.1 to provide the meteorological input fields for the CMAQ. The WRF physics scheme configuration included the Yonsei University (YSU) for the planetary boundary layer (PBL) scheme, the Noah land

surface scheme, the Thompson microphysics scheme, the rapid radiative transfer model for general circulation models (RRTMG) for short and long wave schemes, and the Kain-Fritsch cumulus scheme for cumulus parameterization. 40 vertical layers were setup with the model top pressure at 50 hPa, among which 12 layers were distributed within 1.6 km above the surface. The surface layer thickness was ~50 m. The WRF model was driven by the European Centre for Medium-Range Weather Forecasts (ECMWF) Reanalysis v5 (ERA5) at hourly temporal and 0.25° × 0.25° spatial resolution (Hersbach et al., 2023). To reduce the errors, monthly WRF simulations were divided into six runs, each of which included 12-h spin-up time. Two nested domain simulations were operated with horizontal resolutions of 27 km × 27 km (d01) and 9 km × 9 km (d02) encompassing East Asia and eastern China, respectively. In the CMAQ model, two grids on each WRF lateral boundary were removed, and thus there were 161 × 174 and 233 × 215 grids in d01 and d02, respectively. Figure 1 shows the nested domains configured in the CMAQ as well as the coastal emission control area (CECA) of China covering all the marine waters within 12 nm beyond the territorial baselines.

The CMAQ model was configured to the gas-phase mechanism of Carbon Bond 6 revision 5 (CB6r5) and the aerosol module of AERO7. By modifying the aerosol module and the in-line dust module, two trace elements, V and Ni, were added into the CMAQ as inert aerosol components which only participate in atmospheric physical processes such as diffusion, advection, and deposition. Detailed information on the code modification can be found in the supplementary text (Text S1) and our previous study (Jiang et al., 2024). The initial and boundary conditions for d01 originated from the seasonal average hemispheric CMAQ output from the Community Modeling and Analysis System (CMAS) data repository, while those for d02 were derived from the output data of d01. For the analysis of seasonal variations, the simulations were conducted for January, April, July, and October of 2017 and 2021, representing winter, spring, summer, and autumn, respectively. The annual average was equal to the average of four representative months. To study the impacts under staged fuel oil policies and save computing resources meanwhile, the simulations were operated for each April from 2017 to 2021 based on our previous finding that the impacts of ship emissions in China's coastal areas usually peak in spring (Yu et al., 2021). The spin-up time of each simulation was 5 days. Detailed information on the WRF/CMAQ configuration can be seen in Table 1. The impacts of ship emissions were extracted based on the zero-out method, i.e., two runs with and without ship emissions, named the base run and the exship run respectively in this study.

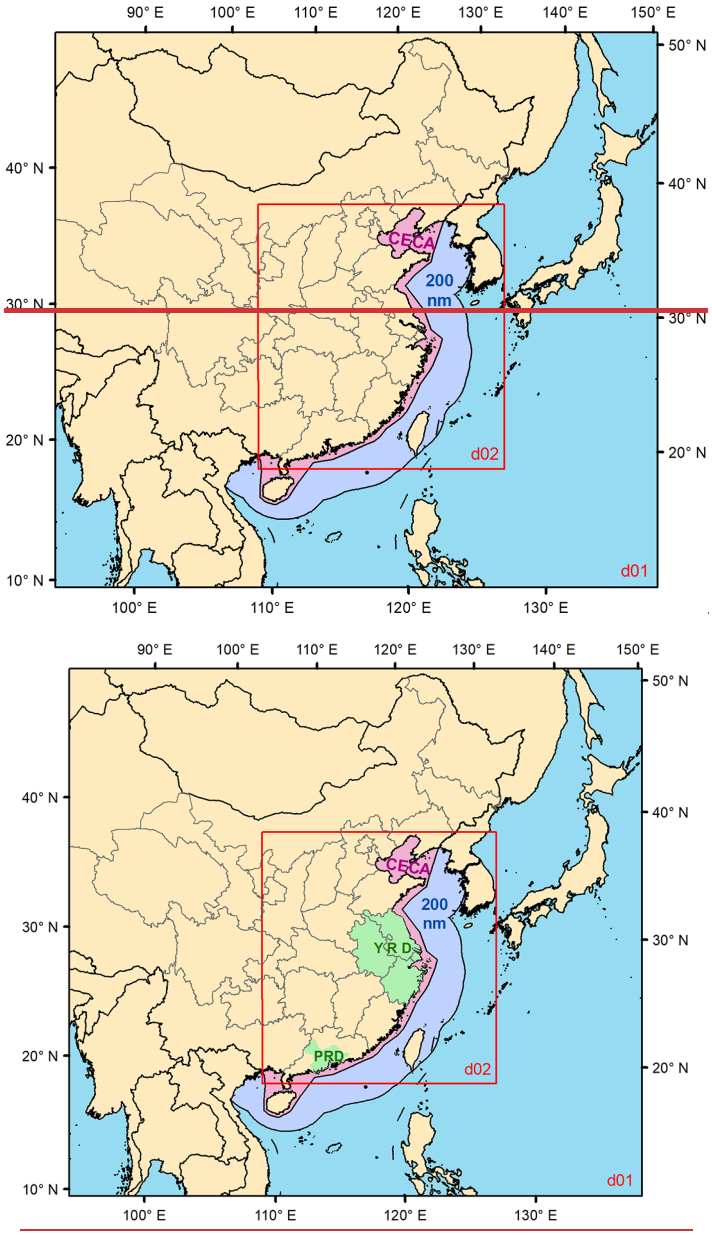

Figure 1. Map of the nested domains configured in the CMAQ. The coastal emission control area (CECA) of China is colored in pink. The boarder of the area within 200 nautical miles (nm) from the coastline of Chinese Mainland is outlined. The Yangtze River Delta (YRD) and the Pearl River Delta (PRD) are colored in green.

Table 1. Details of the WRF/CMAQ configuration.

Simulation period	January, April, July, and October of 2017 and 2021; April of 2018–2020
Grid resolution	27 km × 27 km (d01), 9 km × 9 km (d02)
Vertical layers	40
Surface layer thickness	50 m
Top of model	50 hPa
WRF version 4.1.1	
Grid size	165 (south to north) × 178 (west to east) (d01); 237 × 219 (d02)
Initial/boundary conditions	ERA5 (ECMWF Reanalysis v5), hourly, 0.25° × 0.25°

Microphysics scheme	Thompson
Land surface model	Noah
Planetary boundary layer scheme	YSU (Yonsei University), topo_wind = 2
Cumulus scheme	Kain-Fritsch
Shortwave radiation	RRTMG (Rapid Radiative Transfer Model for General circulation models)
Longwave radiation	RRTMG
Spin-up time	12 h
Number of days per run	6.5*
CMAQ version 5.4	
Grid size	161 × 174 (d01); 233 × 215 (d02)
Initial/boundary conditions	EPA 2017–2018 (d01); output of d01 run (d02)
Gas-phase mechanism	Carbon Bond 6, revision 5 (CB6r5)
Aerosol module	AERO7
Spin-up time	5 days
Number of days per run	36 for January, July, and October; 35 for April

*For WRF, the last run of April is an exception with the time length of 5.5 days.

~~The annual average was equal to the average of four representative months. To study the impacts under staged fuel oil policies and save computing resources meanwhile, the simulations were operated for each April from 2017 to 2021 based on our previous finding that the impacts of ship emissions in China's coastal areas usually peak in spring (Yu et al., 2021). The spin-up time of each simulation was 5 days. Detailed information on the WRF/CMAQ configuration can be seen in Table 1. The impacts of ship emissions were extracted based on the zero-out method, i.e., two runs with and without ship emissions, named the base run and the exship run respectively in this study.~~

2.2 Emission data

2.2.1 Ship emissions

A bottom-up ship emission model based on the AIS data was used to calculate the emission inventories of SO_2 ~~(sulfur dioxide)~~, NO_x, carbon monoxide (CO ~~(carbon monoxide~~), nonmethane volatile organic compounds (NMVOCs) ~~(nonmethane volatile organic compounds~~, ~~PM_{10} (~~PM with a diameter less than 10 μm)(PM_{10}), $PM_{2.5}$, ammonia (NH_3 ~~(ammonia~~), V, and Ni. Detailed information on the setup of the ship emission model ~~and the low-load adjustment multipliers for main engine emission factors (EFs)~~ can be found in the supplementary text (Text S2) and our~~the~~ previous studies (Fan et al., 2016; Feng et al., 2019). In the ship emission model, the power-based EFs under the staged fuel oil policies are categorized by engine type (Table ~~S1~~S2).

During the DECA 1.0 period (2017−2018), we adopted the EFs of various species from Fan et al. (2016) and the fourth IMO Greenhouse Gas (GHG) study. The default setting for main engines (MEs) including slow-speed diesel (SSD) and medium-speed diesel (MSD) engines usually installed for large

vessels was using high sulfur fuel oil (HSFO) with a sulfur content of ~2.7%. A high-speed diesel engine as a main engine (ME_HSD) generally used marine diesel oil (MDO) or marine gas oil (MGO) with a sulfur content of ~0.1%. An auxiliary engine (AE) was assumed to use LSFO with a sulfur content of ~0.5%.

During the DECA 2.0 period (2019), the settings remained the same as those during the DECA 1.0 period in the marine areas outside the CECA. In the CECA, the scenario of EF setting for MEs of large vessels was using LSFO. For the AE, considering that LSFO is often used by sea-going vessels in addition to ULSFO, we took the mean values of the EFs for LSFO and ULSFO.

After the implementation of the IMO Regulation, the settings in all marine areas followed those in the CECA during the DECA 2.0 period. Over land areas, for the sea-going vessels, the EFs of SO_2 and PM for ME were scaled by a factor of 0.2 and 0.26, and 0.315 and 0.391 for AE, respectively, which is due to the implementation of the inland river emission control areas. The EFs of V and Ni for ships navigating in inland waters were lowered by a factor of 10 for the ME due to the nonlinearity between the contents of sulfur and trace elements.

In terms of the EFs of V and Ni for marine vessels during the DECA 1.0 period, we used the values reported in the literature listed in Table ~~S2~~S3. These values during the DECA 2.0 and after 2020 were reduced corresponding to the change ratios reported in our previous study (Yu et al., 2021). The emission inventories of V and Ni were validated through comparison between simulation results and observational data in Shanghai as well as observational data in several coastal cities reported by other studies.

The mapping of $PM_{2.5}$ components from shipping to the AERO7 species is shown in Table ~~S3~~S4. The mass fractions before the IMO Regulation (2017−2019) and after 2020 were referenced from Huang et al. (2018a) and Yang et al. (2022), respectively. The convert factors of NMVOCs emissions from shipping to lumped species in the CB6 mechanism were based on the median VOC profiles from the literature (Table ~~S4~~S5) (Agrawal et al., 2008a; Huang et al., 2018b; Zhang et al., 2024). The initial height of ship emissions considering plume rise and diffusion is basically with the range of 20−100 m (Chosson et al., 2008; He et al., 2021; Badeke et al., 2022; Lansø et al., 2023). We allocated 20% of the sea-going vessel emissions to the surface layer (0−50 m) and 80% to the second layer (50−109 m), while all the inland ship emissions were assigned in the surface layer (Table ~~S5~~S6).

2.2.2 Land-based emissions

For land-based anthropogenic emissions, we used the Multiresolution Emission Inventory for China (MEIC) in 2017−2020 for mainland China and the MIX emission data in 2010 for East Asia excluding mainland China (Li et al., 2017; Zheng et al., 2021). The NH_3 emissions in the MEIC were replaced by the PKU-NH_3 inventory in 2017 (Kang et al., 2016). For natural sources, we used the CAMS-GLOB-BIO v3.1 for monthly global biogenic VOC (BVOC) emissions in 2017−2021 and the biogenic emissions inventory from urban green spaces in China (OUC-BUGS) in 2017−2019 (Sindelarova et al., 2021; Ma et al., 2022). The MEIC, MIX, PKU-NH_3, and OUC-BUGS inventories were downloaded from the website (http://meicmodel.org.cn/). The grid resolutions of MEIC/MIX, BVOC, UBVOC, and PKU-NH_3 are 0.25°, 0.25°, 27 km, and 0.1°, respectively. The $PM_{2.5}$ profiles in Liu et al. (2017a) were used to convert $PM_{2.5}$ from non-shipping emissions to the AERO7 species. We multiplied the $PM_{2.5}$ emissions from the MEIC/MIX by the V and Ni fractions in $PM_{2.5}$ in China by source (Table S3) to obtain the V and Ni emissions from anthropogenic sources excluding shipping (Liu et al., 2018b). The source-specific vertical profiles for industrial, power, residential, and land-based transportation emissions in Table ~~S5~~ S6 were referenced from Zheng et al. (2019).

2.3 Observational data and evaluation of simulation results

The observational data from the national meteorological stations and the national air quality monitoring stations listed in Table ~~S6~~ S7 were used to evaluate the simulation results. The hourly meteorological data were downloaded from the website (http://data.cma.cn), and the hourly air quality data were obtained from China National Environmental Monitoring Center (https://air.cnemc.cn:18014). To evaluate the model performance for $PM_{2.5}$ in coastal areas, 21 port cities along the coast of China were selected as representatives. They rank among the top 20 in terms of cargo or container throughput nationwide and distribute on the coasts of the Bohai Rim (Dalian, Yingkou, Caofeidian, Binhai of Tianjin, and Yantai), the Yellow Sea (Qingdao, Rizhao, and Lianyungang), the Yangtze River Delta (Shanghai, Ningbo, Zhoushan, Hangzhou, Nantong, Zhangjiagang, and Nanjing), the Pearl River Delta (Shenzhen, Guangzhou, and Zhuhai), and the Beibu Gulf (Qinzhou) as well as on the west coast of the Taiwan Strait (Fuzhou and Xiamen). The simulated concentrations in the surface layer were used to compare with the observational data.

We used the hourly observational data from the Pudong site of Shanghai to evaluate the model performance of the tracers of ship emissions (V and Ni) and the secondary inorganic aerosols (SO_4^{2-}, NO_3^-, and NH_4^+). The metallic elements and the ions were measured by the Model Xact 625 (Cooper Environmental Services, LLT, OR, USA) and the MARGA (Model ADI 2080, Applikon Analytical B. V. Corp., The Netherlands), respectively. Detailed information on the location of the monitoring site and the online instruments can be found elsewhere (Yu et al., 2021).

To quantify the model performances of the meteorological factors and the air pollutants, the Spearman's correlation coefficient (r) ~~and~~, the normalized mean bias (NMB), the root mean square error (RMSE), and the index of agreement (IoA) were calculated. ~~for 2-m temperature, wind speed, SO_2, NO_2, O_3 (ozone), and $PM_{2.5}$ at each monitoring station listed in Table A1. The index of agreement (IoA) and the root mean square error (RMSE) were also calculated for the $PM_{2.5}$ component monitoring at the Pudong site.~~

3 Results and discussion

3.1 Changes in ship emissions under the staged fuel oil policies

The emissions of SO_2, NO_x, CO, NMVOCs, $PM_{2.5}$, V, and Ni from shipping in the CECA and inland waters of China from 2017 to 2021 were calculated based on the method introduced in Sect. 2.2.1 (Table 2). NO_x is the major pollutant from shipping, and the nitrogen control policy has not been changed nationwide in the study period. Hence, the amount of NO_x emissions can be regarded as a proxy of ship traffic volume. As mentioned in Sect. 1, the variations of emissions in each April from 2017 to 2021 were used to represent the interannual variations. In the CECA and inland waters of China, the NO_x emissions from shipping gradually increased from 2017 to 2020, with the largest increase (37.1%) from 2017 to 2018, and then slightly decreased in 2021. Due to the increase in ship activities, the NO_x emissions from shipping increased by 51.8% from 2017 to 2021. Figure S1 depicts the spatial distributions of the SO_2 and NO_x emissions from shipping in each April from 2017 to 2021, with high values along the major shipping routes of coastal China, the Yangtze River and its main branches, and the Pearl River. In April 2019, the higher emission intensity on the main route along the southeast coast of China was due to the bypass behavior that ships tend to navigate outside the CECA. For the seasonal patterns, in 2017, the NO_x emissions from shipping were higher in April (114.1 kt) and October (112.1 kt), smaller in July

(101.6 kt) due to the fishing ban, and reached the lowest value in January (89.9 kt) due to the Spring Festival. However, in 2021, the lowest value (128.9 kt) occurred in July, while January exhibited relatively high NO_x emissions (169.2 kt) as the Spring Festival was in February.

By contrast, in the same area, the monthly average SO_2 ($PM_{2.5}$) emissions from shipping decreased by 68.4% (32.8%) from 2017 to 2021 due to the IMO Regulation and China's inland sulfur regulation. The monthly average $PM_{2.5}$ emissions were reduced from 7.6 kt in 2017 to~~.~~ 5.1 kt in 2021. In addition, the monthly average V emissions from shipping experienced a dramatic drop (by 90.8%) from 118.8 t in 2017 to ~~43.9~~11.0 t in 2021. The monthly average Ni emissions decreased from ~~11.0~~41.6 t in 2017 to 24.1~~24.1~~ t in 2021, with a reduction of 42.0%. The average V/Ni ratio decreased from 2.86 in 2017 to 0.46 in 2021. Figure S2 (Figure S3) shows the interannual variations of V (Ni) emissions from shipping and anthropogenic sources excluding shipping. It can be clearly seen that higher V and Ni emissions transferred from nearshore waters to the outer border of the CECA in 2019.

Table S8~~7~~ shows the contributions of ship emissions to the total anthropogenic emissions in China's 200-nm zone and coastal provinces (coastal areas hereafter). The staged low sulfur policies since 2017 significantly reduced the SO_2, V, and Ni emissions, and their reduction rates were larger than those from land-based anthropogenic sources, especially for V. The contributions of ship emissions to the total SO_2, V, and Ni emissions in the coastal areas decreased from 13.9%, 89.2%, and 55.5% in 2017 to 7.7%, 56.0%, and 53.8% in 2021, respectively. The contribution of ship emissions to the total $PM_{2.5}$ emissions in the coastal areas remained at 4.0%. However, the share of NO_x emissions from shipping increased from 13.2% in 2017 to 21.2% in 2021 due to the increase in shipping activities and the reduction in emissions from land-based sources.

Table 2. Time variation of emissions of SO_2, NO_x, CO, NMVOCs, $PM_{2.5}$, V, and Ni from shipping in the coastal emission control area (CECA) and inland waters of China.

	SO_2 (kt)	NO_x (kt)	CO (kt)	NMVOCs (kt)	$PM_{2.5}$ (kt)	V (t)	Ni (t)
January 2017	35.3	89.9	4.2	4.6	6.5	102.1	35.7
April 2017	44.4	114.1	5.4	6.0	8.3	130.7	45.7
July 2017	40.3	101.6	4.6	5.1	7.2	115.0	40.2
October 2017	43.5	112.1	5.3	5.9	8.2	127.4	44.7
April 2018	63.2	156.4	7.3	8.1	11.5	185.9	64.7
April 2019	13.2	166.7	8.1	8.9	5.3	51.1	29.1
April 2020	14.3	170.9	8.1	9.0	5.7	15.3	32.0
January 2021	13.8	169.2	8.2	8.6	5.4	12.1	26.4
April 2021	13.9	164.8	8.0	8.3	5.4	11.8	25.9
July 2021	10.4	128.9	6.1	6.2	4.0	8.2	18.3

October 2021	13.6	171.0	8.4	8.9	5.5	11.7	25.7
2017 average per month	40.9	104.4	4.9	5.4	7.6	118.8	41.6
2021 average per month	12.9	158.5	7.7	8.0	5.1	11.0	24.1

Note: Average per month equals the average of emissions during January, April, July, and October.

3.2 Model performance

Uncertainties in simulation results of air quality can be caused by multiple factors such as the accuracy of meteorological inputs, uncertainties in emission inventories, and the simplification of mechanisms in the model. The model performance of the meteorological elements was acceptable, with negative biases for relative humidity and positive biases for 10-m wind speed in most port cities (Table S9). The simulation results from the base runs were used to evaluate the model performance of the CMAQ model (Table S10). The biases of SO_2 and NO_2 were mainly caused by the uncertainties in local emissions of the MEIC inventory, which impacted on the simulation of secondary pollutants.~~For meteorological elements, as shown in Table S8, the model can outstandingly reproduce the 2-m temperature in each city during the 11 simulated months from 2017 to 2021. Except for Qinzhou (r = 0.88), the r values of the other cities were all above 0.9, and over 0.95 for most cities. The performance for relative humidity was slightly inferior to that of temperature, with correlations ranging from 0.7 to 0.8 in most cities. Except for Dalian (NMB = 2.4%), all other cities show negative biases, which was caused by the underestimation of nighttime radiation cooling. For the 10-m wind speed, overestimation was found in most cities especially megacities such as Shanghai (NMB = 95.5%) and Shenzhen (NMB = 72.2%). The WRF model with a resolution of 9 km can generally reproduce the average wind direction at a station level which is significantly affected by local topography.~~

~~For the concentration of pollutants, the simulation results from the base runs were used to evaluate the model performance of the CMAQ model.~~ The $PM_{2.5}$ concentrations were underestimated in all of the 21 port cities that we concerned, with an average NMB of -31.0% (Fig. 2a), which was mainly attributed to the underestimation of secondary aerosols. Multiple causes such as lack of chemical mechanisms, underestimation of atmospheric oxidants and NH_3 emissions, and overestimation of wind speed may lead to the underestimation of secondary aerosols especially nitrate (Table S11) (Sun et al., 2022; Xie et al., 2022). Nevertheless, the model can reproduce the temporal variation of mean $PM_{2.5}$ concentrations, with a correlation of r = 0.80. The model successfully reproduced the monthly average concentrations of V and Ni as well as the changing impacts of fuel oil policies on V and Ni in Shanghai (Table S12). The

model could characterize the diurnal variation patterns of V, with higher values during the nighttime and lower values during the daytime (Fig. S4). The daily variations of simulation results were more pronounced than those based on observation, which was due to the overestimation of the diurnal cycle of the PBLH using the YSU PBL scheme (Du et al., 2020). The updated V and Ni emissions were verified to be applicable on a national scale by comparing the observational data reported in several other coastal cities and the simulation results in this study (Table S13).

More details on the model performance can be found in Text S3 in the supplement.

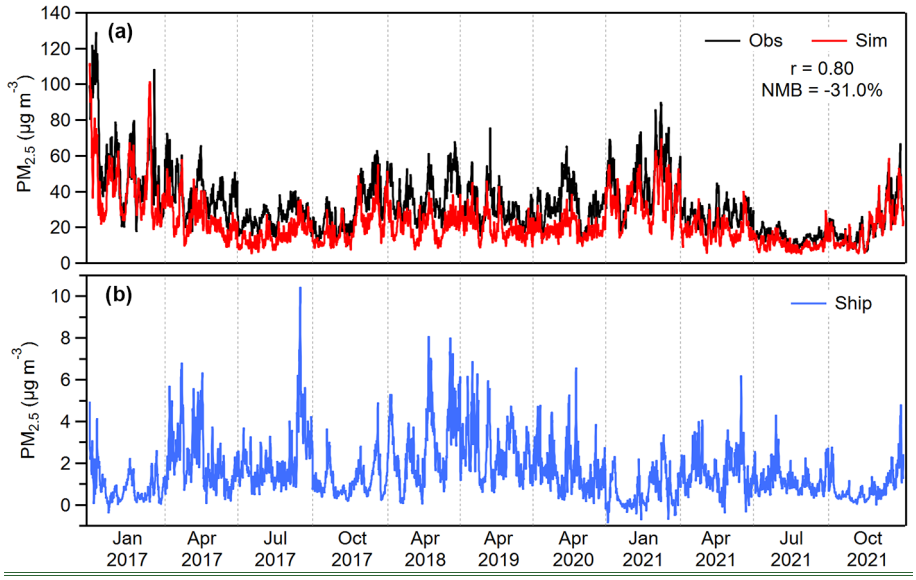

Figure 2. Time series of hourly mean $PM_{2.5}$ concentrations during the simulation periods, averaged for the representative port cities of China: **(a)** observational data (Obs) and simulated results of base runs (Sim), as well as **(b)** simulated shipping-related $PM_{2.5}$.

~~As shown in Table S9, large biases of over ±50% of the concentration levels of SO_2 and NO_2 derived from the CMAQ were found in three megacities including Shanghai, Shenzhen, and Beijing with positive biases, and in Qinzhou with negative biases. These biases were caused by the uncertainties in local emissions of the MEIC inventory. In general, the performance for the daily maximum 8-h average (MDA8) O_3 concentrations in the coastal cities showed the patterns of underestimation in Zhejiang province and to its north and overestimation in Fujian province and to its south, corresponding to the biases of NO_2 concentration. It is noted that the $PM_{2.5}$ concentrations were underestimated in all of the 21 port cities that we concerned, with an average NMB of -31.0% (Fig. 2a), which was mainly attributed to the underestimation of secondary aerosols. For example, the NMB values of the concentrations of~~

~~sulfate, nitrate, and ammonium in Shanghai reached 15.4%, 54.6%, and 21.8% respectively in the entire simulation periods (Table S10). Multiple causes can result in the underestimation of secondary aerosols especially nitrate such as lack of chemical mechanisms, underestimation of daytime O_3 and nighttime relative humidity, as well as overestimation of wind speed (Sun et al., 2022; Xie et al., 2022) . The negative biases were larger in spring, which was likely due to insufficient consideration of heterogeneous reactions like reactions on the surface of mineral dust in the CMAQ model. Nevertheless, the model can reproduce the temporal variation of mean $PM_{2.5}$ concentrations, with a correlation of r = 0.80.~~

For the shipping-related $PM_{2.5}$ concentrations in the concerned port cities, the mean value during the simulation periods was 1.6 μg m^{-3} (Fig. 2b). The hourly mean shipping-related $PM_{2.5}$ peaked on the early morning of 27 July 2017 (local time, hereafter) with a concentration of 10.4 μg m^{-3}, while the minimum value of -0.9 μg m^{-3} occurred on the morning of 2 January 2021. Using the zero-out method may obtain negative shipping-related $PM_{2.5}$ concentrations. Shipping is an emission sector releasing large amounts of NO_x which can participate in complex non-linear chemistry. ~~The limitation of chemical mechanisms in the model could lead to systematic uncertainties.~~ Ship-emitted NO_x significantly consumes atmospheric oxidants such as O_3 and various radicals (OH, HO_2, RO_2, etc.) in areas controlled by the VOC-limited regime. The potential reduction of these oxidants can inhibit the secondary aerosol formation~~, which is the major reason for the~~, resulting in the negative simulated values of $PM_{2.5}$ related to ship emissions. It is noted that the shipping-related $PM_{2.5}$ concentration did not show significant reduction in 2019 compared to 2017 and 2018, which was likely due to the increase in the impact of secondary aerosols (Fig. 2b). This result will be discussed further in Sect. 3.4.1.

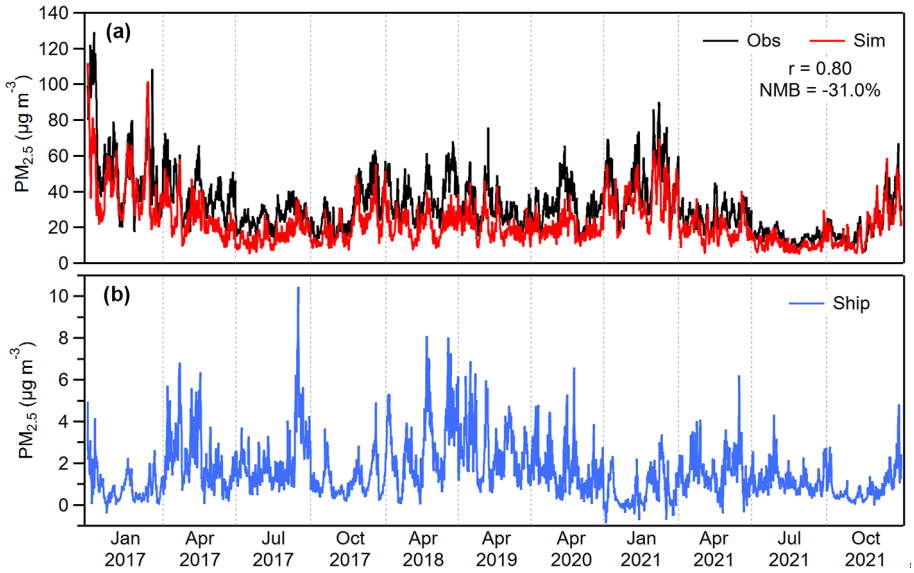

Figure 2. Time series of hourly mean $PM_{2.5}$ concentrations during the simulation periods, averaged for the representative port cities of China: **(a)** observational data (Obs) and simulated results of base runs (Sim), as well as **(b)** simulated shipping related $PM_{2.5}$.

Regarding the tracers of ship emissions, as shown in Table S11, the simulated results of the monthly mean concentrations of V and Ni, as well as the Ni/V ratios are acceptable, thus the emission inventories of V and Ni established in this study being applicable. The model successfully reproduced the changing impacts of fuel oil policies on V and Ni. with higher values during the nighttime and lower values during the daytime. The daily variations of simulation results were more pronounced than those based on observation, which was due to the overestimation of the diurnal cycle of the PBLH using the YSU PBL scheme (Du et al., 2020). For the uncertainties, the model tended to overestimate the concentrations of the two metals in winter, such as overestimating the concentrations of V and Ni in January 2017 by 41% and 30%, respectively. The pattern in July 2021 was underestimating both V and Ni concentrations by 38%. These results can be brought by uncertainties in the simulation of diffusion conditions. The CMAQ model was fed by monthly ship emissions, and the high frequency ship traffic data was smoothed, resulting the relatively weak temporal correlation between observational data and simulation results with hourly resolution. In addition, the uncertainties in meteorology can also affect the simulation of the transport process of ship emissions to urban areas. Nevertheless, the model can characterize the diurnal variation patterns of V (Fig. S4), with higher values during the nighttime and lower values during the daytime. The daily variations of simulation results were more pronounced than those based on observation, which was due to the overestimation of the diurnal cycle of the PBLH using the YSU PBL scheme (Du et al., 2020).

3.3 Spatiotemporal patterns of the ~~shipping-related gas precursors of $PM_{2.5}$~~concentrations of gas precursors from shipping

SO_2 and NO_2 are the key gas precursors of secondary aerosols and the important pollutants from shipping, and thus their spatiotemporal patterns are of interest. As SO_2 is a typical primary pollutant emitted by ships, it was selected to analyze the factors affecting the seasonal and interannual patterns such as emission intensity and meteorological conditions. Regarding the seasonal patterns, the highest SO_2 concentrations from shipping in most regions of China occurred in spring when the prevailing wind was weak and generally blew onshore in the areas with high ship emissions (Fig. S5). Meanwhile, the ship emissions in spring were in a high level with ~8% higher than the annual average. We selected April as the representative month for the analysis of interannual variations nationwide, and thus the policy shifts in advance in some port areas were not considered. In winter, the concentrations on the land showed higher values than those in spring due to the weak diffusion conditions. In the offshore areas, the concentrations in winter were not high as those in spring, which was caused by the significant winter monsoon. The concentrations in summer and autumn were relatively low, which was due to the dilution effect of the southeasterly monsoon in summer and the northeasterly cold air mass in autumn.

As April was selected as the representative month, the interannual variations of ~~Figure 3 depicts the impacts of ship emissions~~the ~~on the~~ SO_2 and NO_2 concentrations from shipping ~~during the DECA 1.0 period (represented by 2017) and after the implementation of the IMO Regulation (represented by 2021)~~in each April from 2017 to 2021 are shown in Fig. 3~~.~~. To study the general interannual variations during the policy stages, the 99th percentile (P_{99}) values of the grids in the model domain were used in the following and very high values on a local scale were not considered. The overall changes in the impact of ship emissions on the air pollutants by annual average from 2017 to 2021 can be found in the supplement (Text S4).

The SO_2 concentrations from shipping experienced evident staged reduction. The P_{99} values from 2017 to 2021 were 4.1, 5.2, 2.6, 1.5, and 1.2 μg m^{-3} in the chronological order. Comparing the concentrations in 2018 and 2019, it was found that the DECA 2.0 had the effect of halving the SO_2 concentrations from shipping. After 2020, hotspots with values over 4 μg m^{-3} were only found along the coast of Zhejiang with dense fishing activities. The P_{99} value in 2021 was even lower than that in 2020, which was related to the rebounce of fishing activities after the COVID-19 lockdown in early 2020. Comparing the P_{99}

values in 2019 and 2021, a reduction rate of 53.8% was obtained due to the IMO Regulation and was comparable with that brought by the DECA 2.0. In Sect. 3.3 and Sect. 3.4, the effect evaluation for the DECA 2.0 was based on the difference between 2019 and 2018, while that for the IMO Regulation were based on the difference between 2021 and 2019. In the studied five years, the SO_2 concentrations from shipping over the Yellow Sea exhibited the lowest level in 2020, which was attributed to the decline of long-distance shipping between China and Korea as well as between southern and northern China caused by the COVID-19 lockdown. ~~With a remarkable decrease in fuel sulfur content (FSC) globally, the SO_2 concentration from shipping reduced in all simulated areas (Fig. 3c). The largest reduction was observed in the lower reaches of the Yangtze River reaching 5.2 μg m^{-3} due to the fuel type shift to the ULSFO.~~

~~In 2017, the spatial pattern of the SO_2 concentration from shipping performed high values along the main routes with the maximum value of 6.1 μg m^{-3} (in a grid cell level) in the Yangtze River Estuary (YRE), and a decreasing trend toward both sides (Fig. 3a). In 2021, the hotspots in China's coastal areas were located to the east of Shanghai and Zhejiang, to the southeast of Fujian, and in the Pearl River Estuary (PRE), with the highest value of 2.5 μg m^{-3} (Fig. 3b). With a remarkable decrease in fuel sulfur content (FSC) globally, the SO_2 concentration from shipping reduced in all simulated areas (Fig. 3c). The largest reduction was observed in the lower reaches of the Yangtze River reaching 5.2 μg m^{-3} due to the fuel type shift to the ULSFO.~~

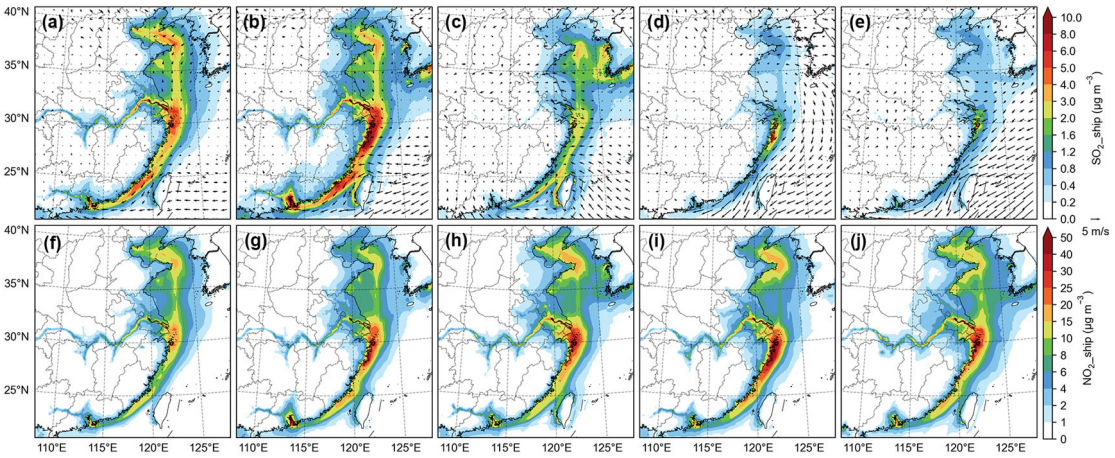

Figure 3. Impacts of ship emissions on **(a–e)** the SO_2 concentrations (SO_2_ship) and the simulated monthly average wind fields as well as **(f–j)** the NO_2 concentrations (NO_2_ship) in April from 2017 to 2021 in the chronological order from left to right.

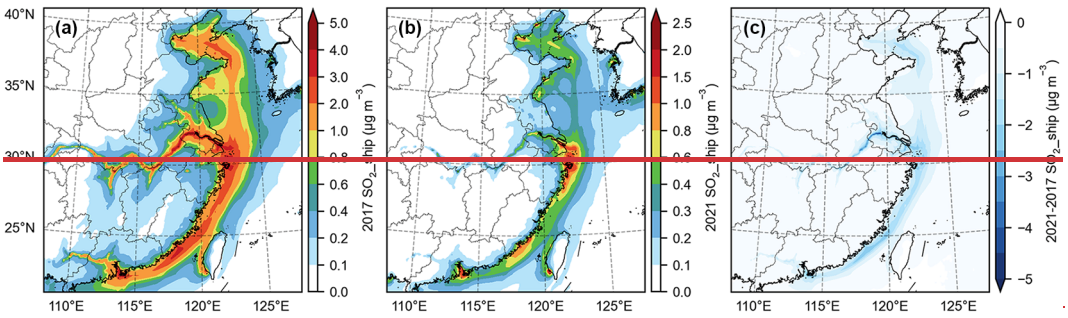

Figure 3. Impacts of ship emissions on the SO_2 concentrations (SO_2_ship) in **(a)** 2017 and **(b)** 2021, as well as its **(c)** absolute change from 2017 to 2021. The annual average equals the average of January, April, July, and October here and hereafter.

As SO_2 is a typical primary pollutant emitted by ships, it was selected to analyze the factors affecting the seasonal and interannual patterns such as emission intensity and meteorological conditions. With respect to the seasonal patterns, the highest SO_2 concentrations from shipping in most regions of China occurred in spring when the prevailing wind was weak and generally blew onshore in the areas with high ship emissions (Fig. S5). Meanwhile, the ship emissions in spring were in a high level with ~ 8% higher than the annual average. Hence, we selected April as the representative month for the analysis of interannual variations. In winter, the concentrations on the land showed higher values due to the weak diffusion conditions. In the offshore areas, the concentrations in winter were not high as those in spring, which was caused by the significant winter monsoon. In summer, despite the better diffusion conditions, the concentrations in the areas with dense ship emissions were only second to those in spring in 2017. However, the concentrations shared relatively low levels in summer and autumn in 2021. This difference can be attributed to the direction and the intensity of the summer monsoon. In the summer of 2021, the strong southeasterly wind was in favor of the diffusion of ship emissions. Although the ship emissions in autumn were comparable to those in spring, the concentrations in autumn were much lower than those in spring in marine areas, which was resulted from the northeasterly prevailing wind diluting the pollutants emitted by ships.

Figure S6 shows the variations of the SO_2 concentrations from shipping in each April from 2017 to 2021. The overall concentrations experienced staged reduction with the changes of the fuel oil policies. However, due to large variations in local emissions, the maximum value in each year presented a fluctuating trend with 7.3, 30.1, 7.1, 11.4, and 4.3 μg m^{-3} from 2017 to 2021. The hotspots located in the central part of the coast of Zhejiang in 2018 and 2020 were likely due to the intensive fishing activities. Besides, the simulated wind field patterns in the coastal areas were similar in April of 2017, 2018, 2019,

and 2021. However, in April 2020, a stable high-pressure system over the Yellow Sea led to a better horizontal diffusion condition for the emissions on the main routes.

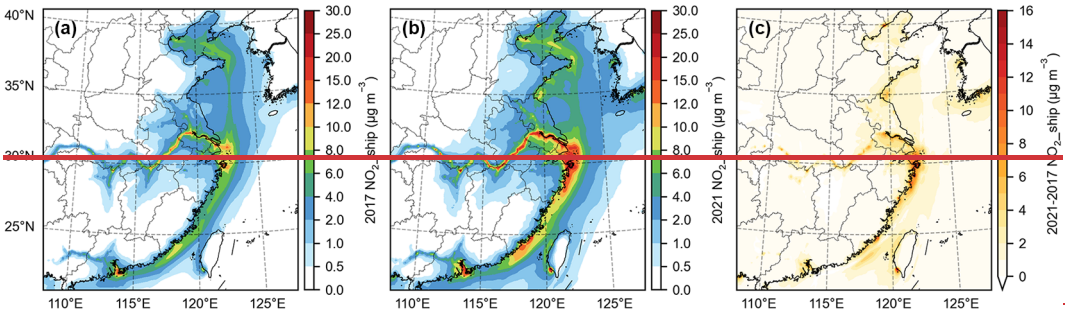

Figure 4. Impacts of ship emissions on the NO_2 concentrations (NO_2_ship) in **(a)** 2017 and **(b)** 2021, as well as its **(c)** absolute change from 2017 to 2021.

The main source of the ambient NO_2 from shipping is the rapid oxidation of NO in ship plumes, and the high concentrations still fixed on the main routes and ports in the lower reaches of the Yangtze River and the PRE, as well as coastal Shanghai, Zhejiang, and Fujian (Fig. 4). The P_{99} values in April from 2017 to 2021 were 14.1, 18.0, 18.8, 20.8, and 18.3 μg m^{-3} in the chronological order. The impacts of the staged policy shifts on the P_{99} values were within ±5%. The maximum values in 2017 and 2021 were 17.9 and 26.0 μg m^{-3}, respectively. The concentrations increased in most areas from 2017 to 2021, and the increase was larger near the ports of Ningbo-Zhoushan in Zhejiang, Quanzhou in Fujian, Gaoxiong in Taiwan, and Tangshan in Hebei with the maximum of 15.4 μg m^{-3}. The decrease in SO_2 and the increase in NO_2 were both significant from 2017 to 2021, which is are expected to affect the formation pathways of shipping-related secondary aerosols and the composition of shipping-related $PM_{2.5}$.

3.4 Spatiotemporal patterns of shipping-related $PM_{2.5}$ and its components

3.4.1 Fine particulate matter ($PM_{2.5}$)

$PM_{2.5}$ related to ship emissions contains primary and secondary aerosols, and secondary aerosols lead to the difference in the spatial spatiotemporal patterns between the gas precursors and $PM_{2.5}$. Figure 4 shows the interannual variations of the shipping-related $PM_{2.5}$ concentrations in the spring of 2017−2021. The P_{99} value in the model domain in April 2017 was 4.1 μg m^{-3} and slightly increased to 4.6 μg m^{-3} in April 2018. The increase was relatively significant over the PRE and the coastal waters of Zhejiang, which was due to the increase in shipping activities.

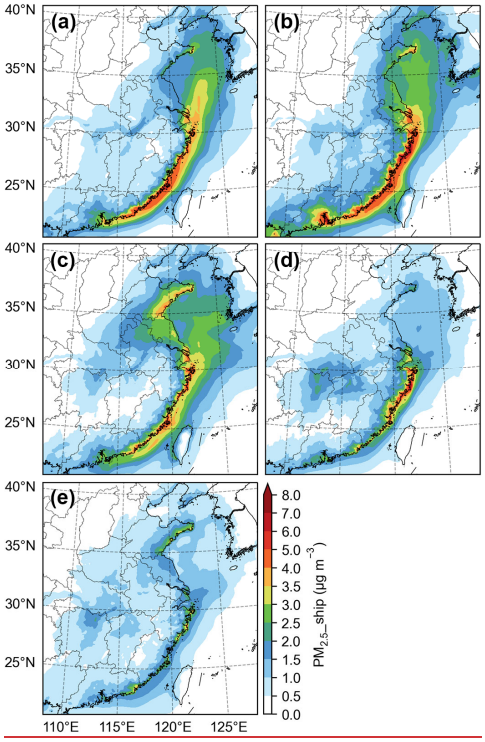

Figure 4. Interannual variations of the potential impacts of ship emissions on $PM_{2.5}$ ($PM_{2.5}$_ship) concentrations in April of **(a)** 2017, **(b)** 2018, **(c)** 2019, **(d)** 2020, and **(e)** 2021.

Owing to the DECA 2.0 policy, in April 2019, the P_{99} value was reduced to 3.7 μg m^{-3}, with a reduction rate of 19.5% year on year. This reduction rate was significantly lower than that of the primary $PM_{2.5}$ emissions from shipping (53.8%). There was even an increase along the coast of Shandong province. It was found that high values were closer to the coastline during the DECA 2.0 period compared to the DECA 1.0 period. This pattern was similar to the shipping-related NO_3^- and NH_4^+ which can be seen in Sect. 3.4.3. In NH_3-rich port areas, the increasing NO_x emissions from shipping resulted in more nitrate formation. Meanwhile, the reduction in the SO_2 emissions provided more opportunities for HNO_3 to react with NH_3. Besides, the difference between the shipping-related $PM_{2.5}$ concentrations inside and outside the CECA border was much smaller compared to the SO_2 concentrations from shipping, which was due to the onshore transport of aged aerosols from marine areas outside the CECA where high-sulfur fuel oils were still used. These aged aerosols could also contribute to the shipping-related $PM_{2.5}$ in the port cities. Therefore, the impact of secondary aerosols partly offset the effect of primary PM emission reduction during the DECA 2.0 period.

In April 2020, due to the IMO Regulation, the P_{99} value decreased to 3.3 μg m^{-3}. The concentrations declined in most marine areas especially the Yellow Sea in which the main routes were not included in

the CECA before 2020. In April 2021, ship emissions were more evenly distributed as the pandemic impact was limited. The concentrations of shipping-related $PM_{2.5}$ only presented relatively high values in a city level, with the P_{99} value of 2.4 μg m^{-3} in coastal Zhejiang. Comparing the P_{99} values in 2021 and 2019, a reduction rate of 35.6% was achieved due to the policy shift from the DECA 2.0 to the IMO Regulation.

~~As shown in Fig. 5a, the concentrations of shipping related $PM_{2.5}$ in 2017 displayed values of over 2 μg m^{-3} along the main routes from the Yellow Sea to coastal Fujian, with the maximum of 3.8 μg m^{-3} near Zhoushan Islands. The areas with concentration over 1 μg m^{-3} covered most of the Yellow and Bohai Seas and extended to the Middle Yangtze River (~ 1000 km away from the coast). However, the areas with concentration over 1 μg m^{-3} shrunk to the coast and the central Yangtze River Basin in 2021, with the maximum of 2.6 μg m^{-3} in the eastern Shandong Peninsula (Fig. 5b). The areas with shipping related $PM_{2.5}$ of over 0.1 μg m^{-3} occupied most of the model domain both in 2017 and 2021, which was markedly different from the patterns of SO_2 and NO_2 from shipping. This result is caused by sustained aging processes during the transport of ship-emitted pollutants as well as the longer lifetime of PM compared to SO_2 and NO_2 (Seinfeld and Pandis, 2016). The decrease in the concentration of shipping-related $PM_{2.5}$ showed the largest value of 1.9 μg m^{-3} in the sea area of Zhoushan Islands, while the slight increase within 0.5 μg m^{-3} was found in very small areas in Hunan, Shandong, and Liaoning provinces (Fig. 5c).~~

The result in Lv et al. (2018) showed that the increased $PM_{2.5}$ concentration in China caused by shipping was up to 5.2 μg m^{-3} in 2015. The values in this study were 3.8 μg m^{-3} in 2017 and 2.6 μg m^{-3} in 2021, demonstrating the decreasing trend of the shipping-related $PM_{2.5}$ concentrations under the staged fuel oil policies in China (Fig. S6).

Figure 5 shows the interannual variations of the contributions of ship emissions

~~For the relative potential impact of ship emissions on $PM_{2.5}$, also called the contribution of ship emissions~~ to ambient $PM_{2.5}$ concentrations~~, in 2017,~~. The P_{99} values in April from 2017 to 2021 were 26.7%, 29.3%, 34.3%, 22.2%, and 17.2% in the chronological order. It is of interest that the contributions near the coast of China in 2019 were even higher than those in 2018 although the concentrations were lower in 2019. These high values in 2019 were related to the increase in the shipping-related $PM_{2.5}$ concentrations outside the CECA border as well as the decrease in the $PM_{2.5}$ concentrations related to land-based sources. Lower values in remote marine areas were related to the contribution of sea salt (Fig. S7).

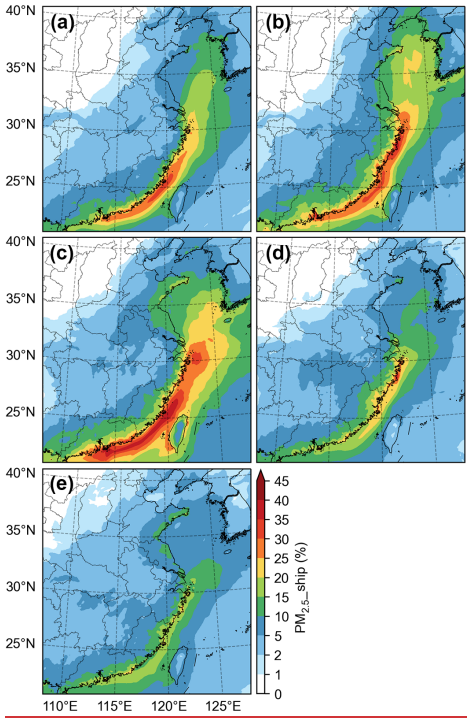

Figure 5. Interannual variations of the contributions of ship emissions to $PM_{2.5}$ concentrations ($PM_{2.5}$_ship%) in April of **(a)** 2017, **(b)** 2018, **(c)** 2019, **(d)** 2020, and **(e)** 2021.

The seasonal patterns of the absolute and relative impacts of ship emissions on $PM_{2.5}$ are shown in Fig. S8. The shipping-related $PM_{2.5}$ concentrations exhibited higher values in summer and spring while lower values in autumn and winter, which was different from those of the SO_2 and NO_2 concentrations from shipping. The key factor was the conversion rates of gas precursors to secondary aerosols. In summer, despite the better diffusion conditions, hotspots were found in coastal marine areas, which was likely due to secondary organic aerosol (SOA) formation (see Sect. 3.4.4). In winter, it is worth noting that the values in most northern China did not exceed 0.5 μg m^{-3} and even lower than 0.1 μg m^{-3} in some coastal areas, which was very different from the pattern of SO_2 from shipping. NH_3 is consumed by SO_2 and NO_x from land-based emissions in prior to ship emissions, and thus the formation of secondary aerosols related to shipping is inhibited, which called the domination effect by land-based sources. Regarding the relative impact of shipping-related $PM_{2.5}$, the seasonal pattern generally showed a decreasing trend in summer, spring, autumn, and winter in the model domain, which was mainly due to the impact of the East Asian monsoon on the relative spatial distribution of ship and land-based emissions.~~larger values of over 10% distributed along the main routes from the southern Yellow Sea to the northern South China Sea, with the maximum of 21.3% in the Taiwan Strait (Fig. 5d). The distance between the land areas with~~

~~the relative impact of over 4% and the coast could be up to ~300 km. The relative impact was not less than 1% in the model domain except for northwestern China. Lower values in remote marine areas were related to the contribution of sea salt. In 2021, the relative impact values exceeding 10% were found only along China's southeast coast and in the eastern end of Shandong Peninsula, with the maximum of 16.9% (Fig. 5e). In the areas with high relative impact values mentioned above, the relative impact decreased remarkably, with the largest decrease of -11.0 percentage points (Fig. 5f). However, an increase in the relative impact was observed near the south and east coast of Shandong with the maximum of 3.4%, and small positive changes scattered in China's inland areas. This result may be caused by the increase in nitrate formation related to shipping and the decrease in land-based anthropogenic emissions, which will be discussed in Sect. 3.4.3.~~

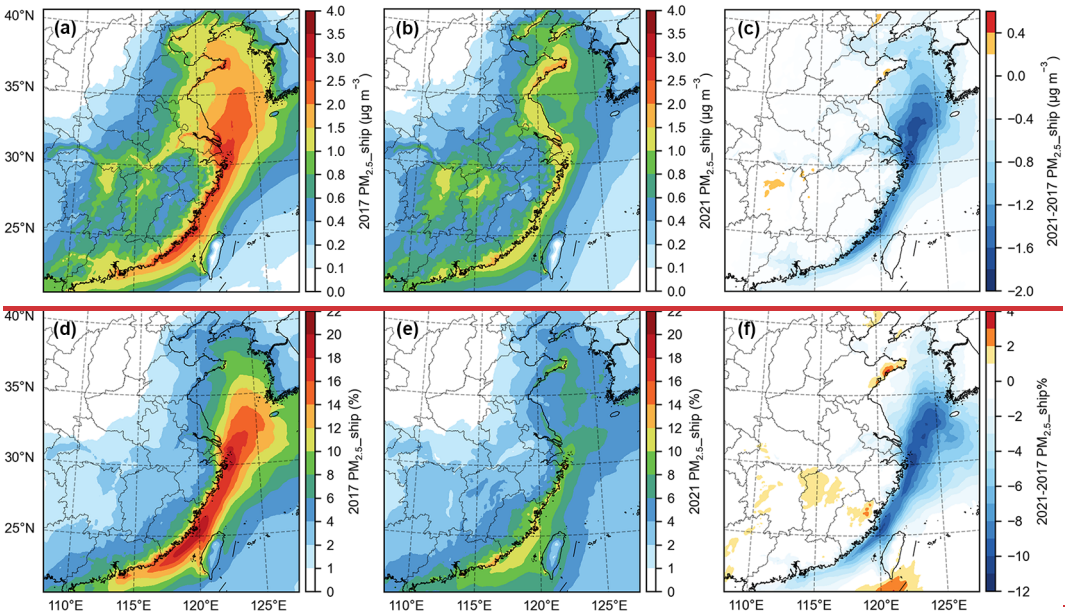

~~**Figure 5.** Potential impacts of ship emissions on $PM_{2.5}$ ($PM_{2.5}$_ship): for concentration (in μg m^{-3}) in **(a)** 2017 and **(b)** 2021, as well as **(c)** the absolute change from 2017 to 2021; and for contribution (in %) in **(d)** 2017 and **(e)** 2021, as well as **(f)** the change of percentage from 2017 to 2021 (in percentage point).~~

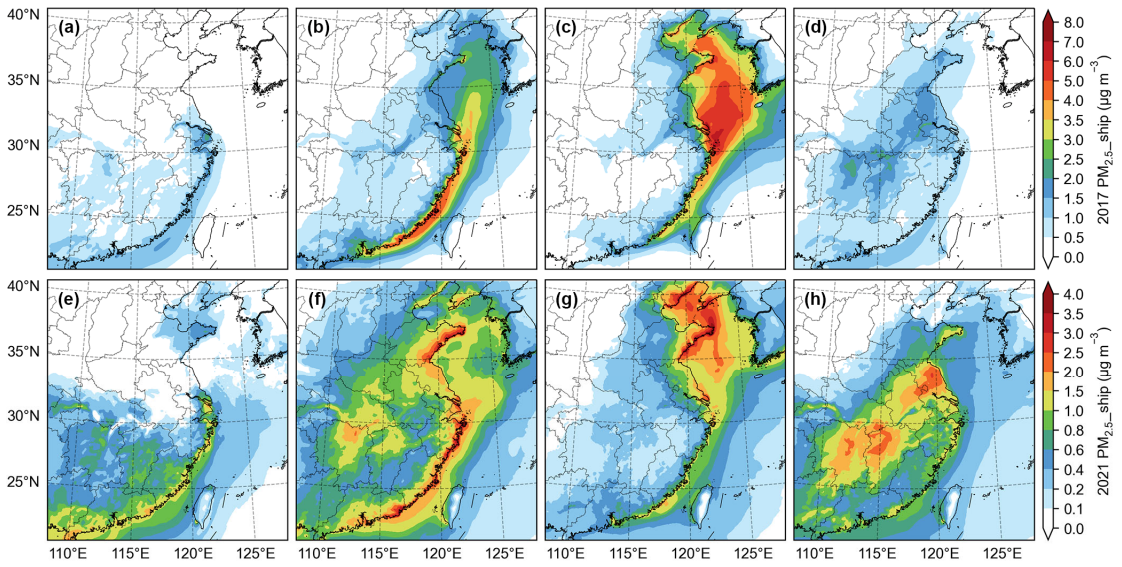

Figure 6. Seasonal patterns of the potential impacts of ship emissions on $PM_{2.5}$ ($PM_{2.5}$_ship) concentrations in **(a)** January, **(b)** April, **(c)** July, and **(d)** October of 2017; and **(e)** January, **(f)** April, **(g)** July, and **(h)** October of 2021.

~~The seasonal patterns of the concentrations of shipping related $PM_{2.5}$ in 2017 and 2021 were rather different from those of the SO_2 and NO_2 concentrations from shipping (Fig. 6). During the springtime, relatively high shipping related $PM_{2.5}$ concentration was located along the southeast coast both in 2017 and 2021 as well as the coast of Shandong in 2021. The pollutants emitted by ships were prone to accumulate due to the meteorology and experience chemical reactions in coastal areas in spring. Unexpectedly, the hotspots transferred to sea areas in summer, and the maximum values were even higher than those in spring for both years. As the diffusion conditions are better in summer, there should be other factors like secondary organic aerosol (SOA) formation (see Sect. 3.4.4).~~

~~In autumn, cold air masses from northeastern Asia diluted the gas precursors in coastal areas. The atmosphere over inland areas were in an ammonia rich condition favoring nitrate formation, and thus relatively high values shifted to inland areas. During the wintertime, the shipping-related $PM_{2.5}$ concentration showed moderate levels in Shanghai both in 2017 and 2021, as well as along the southeastern to southern coast in 2021. It is worth noting that the values in most northern China did not exceed 0.5 μg m^{-3} and even lower than 0.1 μg m^{-3} in some coastal areas, which was very different from the pattern of SO_2 from shipping. Weaker diffusion conditions and lower temperature as well as higher nocturnal humidity led to higher efficiency of secondary aerosol formation. However, NH_3 is sufficiently consumed by SO_2 and NO_x from land based emissions, and thus the formation of secondary aerosols related to shipping is inhibited, which called the competitive mechanism by land-based sources. As~~

discussed in Sect. 3.3, meteorology is a much more important factor affecting the seasonal patterns of the SO_2 and NO_2 concentrations from shipping compared to emissions. However, the conversion rate of gas precursors is a key factor affecting the seasonal pattern of the concentration of shipping-related $PM_{2.5}$, while the influence of diffusion conditions is relatively small.

For the relative impact of shipping-related $PM_{2.5}$, the seasonal pattern generally showed a decreasing trend in summer, spring, autumn, and winter in the model domain, which was mainly due to the impact of the East Asian monsoon on the relative spatial distribution of ship and land-based emissions (Fig. 7). Despite the fact that the concentration of shipping-related $PM_{2.5}$ in coastal areas peaked in spring, the highest relative impact was recorded in summer. In the summer of 2017, the largest relative impact exceeded 50% and 25% over the marine and land areas of the southeastern coastal areas, respectively. In the summer of 2021, the areas with higher absolute and relative impacts of shipping-related $PM_{2.5}$ shifted northward to the Yellow Sea, which was driven by the southeasterly summer monsoon. Among the concerned port cities, in the summer of 2017, Zhoushan showed the highest value of 37.6%, while the lowest value of 4.8% for Qinzhou. In the summer of 2021, the highest (25.0%) and the lowest values (4.2%) occurred in Zhoushan and Nanjing, respectively. In comparison, the relative impact was much smaller in winter, with the highest value of 5.7% in Ningbo and the lowest value of 0.14% in Caofeidian in the winter of 2017, and the highest value of 6.2% in Fuzhou and the lowest value of 0.04% in Nanjing in the winter of 2021.

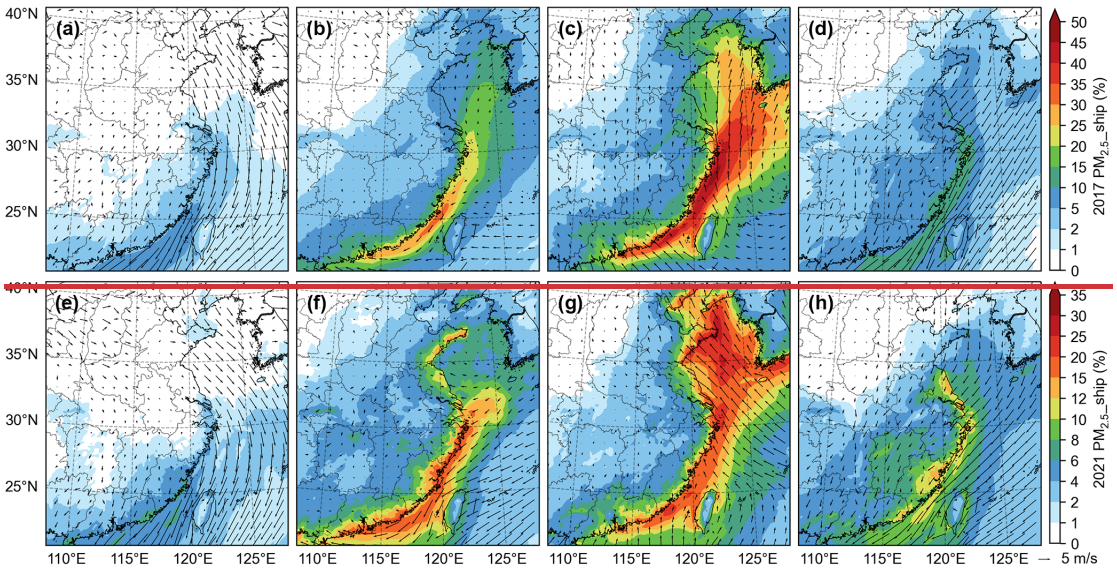

Figure 7. Seasonal patterns of the potential impacts of ship emissions on $PM_{2.5}$ ($PM_{2.5}$_ship) for contribution as well as the simulated monthly average wind fields in **(a)** January, **(b)** April, **(c)** July, and **(d)** October of 2017; and **(e)**

~~January, **(f)** April, **(g)** July, and **(h)** October of 2021.~~

~~Figure 8 shows the spatial patterns of the concentration of shipping related $PM_{2.5}$ in the spring of 2017–2021. In April 2017, the highest concentration of 7.2 μg m^{-3} was located over the coastal waters of Fujian. In April 2018, the highest concentration rose to 10.4 μg m^{-3}; the concentration generally increased in the model domain, especially over the PRE and the coastal waters of Zhejiang, which was due to the increase in shipping activities. In April 2019, high values were closer to the coastline compared to the DECA 1.0 period, and the CECA border was indistinct compared to the pattern of the SO_2 concentration from shipping. This result highlights the crucial role of secondary aerosols in the shipping-related $PM_{2.5}$ in the presence of plenty NH_3 emissions. The highest concentration reduced to 6.5 μg m^{-3}, whereas there was an increase along the coast of Shandong due to more secondary aerosol formation. In April 2020, due to the implementation of the IMO Regulation, the concentration declined in most marine areas especially the Yellow Sea in which the main routes are not included in the CECA before 2020. However, the concentration increased along coastal Zhejiang, and the highest value in the model domain rebounced to 8.3 μg m^{-3}, which was in accord with the patterns of the SO_2 and NO_2 concentrations from shipping. This result was likely due to the recovery of fishing activities after the COVID-19 lockdown. In April 2021, ship emissions were more evenly distributed, and hence the concentration of shipping related $PM_{2.5}$ only presented relatively high values in a city level, with the maximum of 4.5 μg m^{-3} in coastal Zhejiang.~~

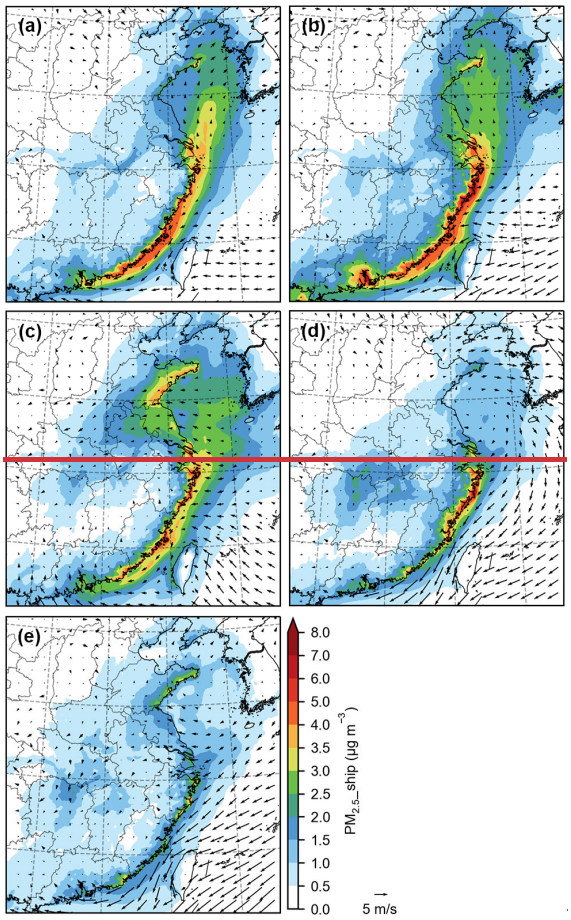

~~**Figure 8.** Interannual variations of the potential impacts of ship emissions on $PM_{2.5}$ ($PM_{2.5}$_ship) concentrations as well as the simulated monthly average wind fields in April of **(a)** 2017, **(b)** 2018, **(c)** 2019, **(d)** 2020, and **(c)** 2021.~~

3.4.2 Trace elements (V and Ni)

V and Ni are strongly correlated with SO_2 among the chemical species emitted by ships, and thus their concentrations from shipping share similar ~~spatial~~ spatiotemporal patterns (Fig. 7). ~~In the CMAQ model, V and Ni do not participate in any chemical reactions, while SO_2 can be oxidized to sulfuric acid (H_2SO_4) and sulfate. Therefore, emissions and meteorology are the factors affecting the concentrations of $PM_{2.5}$-bound V and Ni from shipping.~~ In the model domain, the P_{99} values of the $PM_{2.5}$-bound V(Ni) concentrations from shipping in April from 2017 to 2021 were 18.1(5.6), 23.8(7.4), 13.3(5.0), 2.7(5.0), and 2.1(3.9) ng m^{-3} in the chronological order. The reduction rate of the V (Ni) concentrations from shipping caused by the policy shift from the DECA 1.0 to 2.0 was 44.1% (33.3%), while a further reduction rate of 84.5% (21.6%) was achieved due to the IMO Regulation. The relative changes of the V and Ni concentrations from shipping were different. The V/Ni ratios in ambient particles from shipping decreased from ~3.0 to ~0.5 from 2017 to 2021. ~~In 2017, the areas with the V concentration from shipping exceeding 0.5 ng m^{-3} covered most parts of eastern China, with the maximum of 24.5 ng m^{-3} (Fig. 9a).~~

~~In contrast, for the land areas, only coastal areas and the Yangtze River showed values over 0.1 ng m^{-3} in 2021, and the maximum along the coast substantially decreased to 2.2 ng m^{-3} (Fig. 9b). Ship emissions overwhelmingly dominated the V concentration in the marine and coastal areas as well as along the Yangtze River in 2017 (Fig. 9c). However, in 2021, the contribution of land-based emissions was closed to or even higher than that of ship emissions in the coastal areas (Fig. 9d). There was also an evident decrease in the contribution of ship emissions in remote marine areas because V from land-based emissions including anthropogenic sources and mineral dust can be transported by the high-altitude westerly wind.~~

~~The spatial pattern of the Ni concentration from shipping was similar to that of the V concentration from shipping, while their relative changes from 2017 to 2021 were different (Fig. 10). The highest Ni concentration from shipping was 7.8 ng m^{-3} in 2017 and decreased to 4.1 ng m^{-3} in 2021. The V/Ni ratios in ambient particles from shipping decreased from ~3.0 to ~0.5 from 2017 to 2021. In 2017, the contribution of ship emissions to the Ni concentration was lower compared to V. Over land areas, the contour of 80% for the V concentration share generally corresponded to the contour of 40% for the Ni concentration share. It is noted that the reduction in the Ni concentration share from 2017 to 2021 was small in the model domain, and the Ni concentration share overtook the V concentration share.~~ Despite the sharp reduction in the concentrations of V and Ni from shipping, shipping is still an important source of the ambient V and Ni under the current fuel oil regulations. The contributions of ship emisisons to the concentrations of V and Ni could exceed 50% along the coast in 2021 (Fig. S9 and Fig. S10).

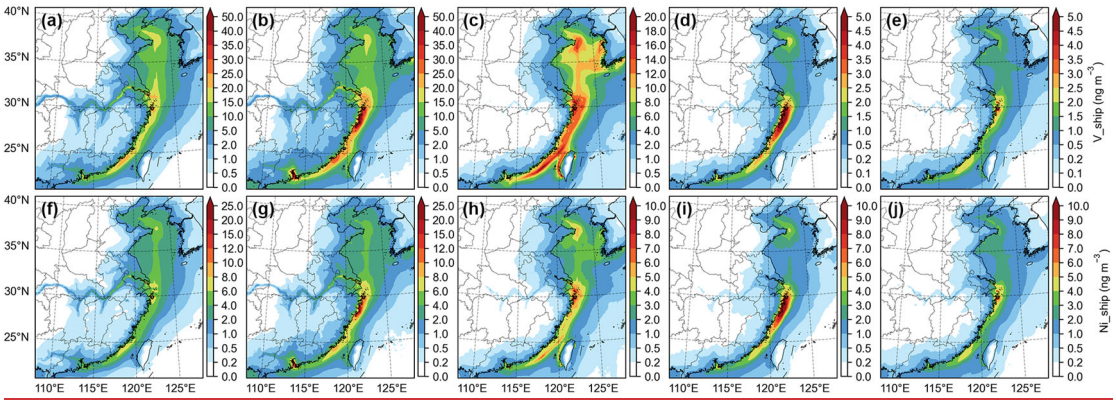

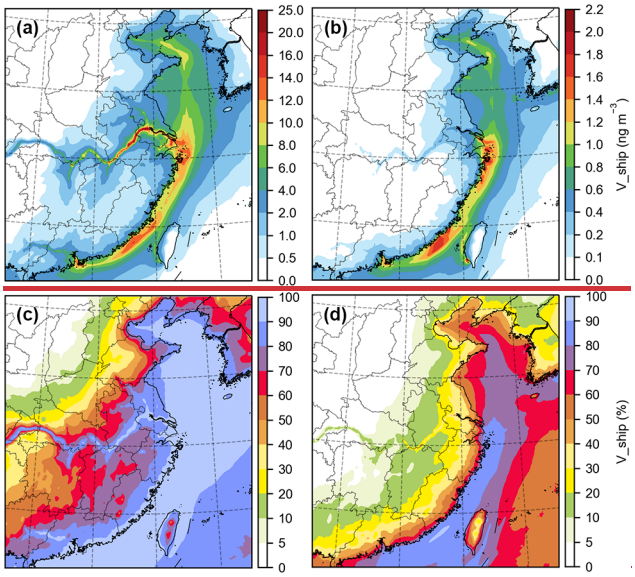

Figure 7. Impacts of ship emissions on **(a–e)** the V concentrations (V_ship) and **(f–i)** the Ni concentrations (Ni_ship) in April from 2017 to 2021 in the chronological order from left to right.

~~**Figure 9.** Impacts of ship emissions on V (V_ship): for concentration (in ng m^{-3}) in $PM_{2.5}$ in **(a)** 2017 and **(b)** 2021; and for contribution (in %) in **(c)** 2017 and **(d)** 2021.~~

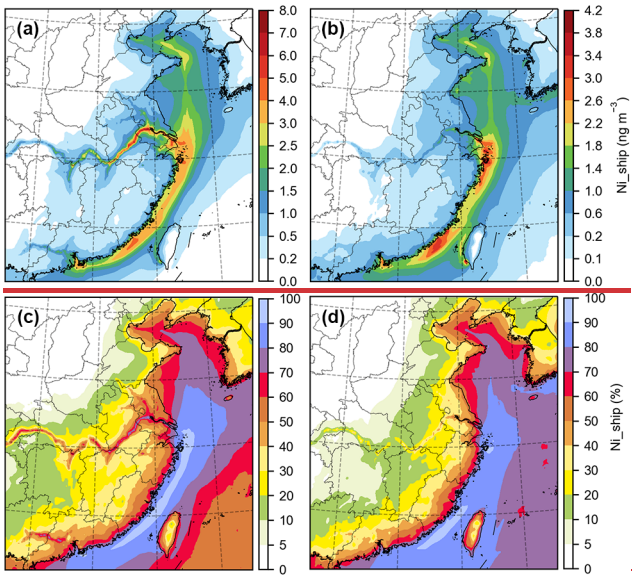

~~**Figure 10.** Impacts of ship emissions on Ni (Ni_ship): for concentration (in ng m^{-3}) in $PM_{2.5}$ in **(a)** 2017 and **(b)** 2021; and for contribution (in %) in **(c)** 2017 and **(d)** 2021.~~

3.4.3 Secondary inorganic aerosols

Sulfate (SO_4^{2-}), nitrate (NO_3^-), and ammonium (NH_4^+), known as SNA for short, are the most important secondary inorganic species in $PM_{2.5}$. Their concentrations are highly related to the concentrations and the conversion rates of the gas precursors including SO_2, NO_x, and NH_3. Their spatiotemporal variations

are shown in Fig. 8-. Given that $PM_{2.5}$ especially secondary species like nitrate was underestimated in China's coastal cities in this study as discussed in Sect. 3.2, the simulated concentrations of SNA related to ship emissions were conservative.

For the formation of sulfate, the main atmospheric oxidant is hydroxyl radical (OH) which transforms SO_2 to H_2SO_4. Then, H_2SO_4 is neutralized by NH_3 forming $(NH_4)_2SO_4$, or dissolves in aerosol liquid water and binds with positive ions like Na^+. As EC is a stable species, the primary sulfate concentration from shipping can be calculated through multiplying the EC concentration from shipping by the ratio of SO_4^{2-} to EC in ship-emitted PM in Table S4. Thus, the secondary part of shipping-related sulfate equals the difference of the total concentration and the primary part. Based on this assumption, it was found that primary sulfate emitted by ships played a minor role while secondary sulfate accounted for 80%–90% of the shipping-related sulfate regardless of the policy shift.

The P_{99} values of the shipping-related sulfate concentrations from 2017 to 2021 were 1.5, 1.8, 1.5, 0.5, and 0.5 μg m^{-3} in the chronological order. Due to the policy shift from the DECA 1.0 to 2.0, the P_{99} value of the sulfate concentrations only decreased by 15.8%, and the decrease rate was significantly lower compared to the SO_2 concentrations (49.7%). During the DECA 2.0 period, the SO_2 emissions outside the CECA were still at a high level and had the potential to generate sulfate in the onshore transport processes, which partly offset the impact of SO_2 emission reduction in the CECA. The P_{99} value of the sulfate concentrations was then reduced by 66.1% due to the policy shift from the DECA 2.0 to the IMO Regulation. After 2020, the SO_2 emissions outside the CECA sharply decreased, and the offset effect no longer existed.~~For the formation of sulfate, the main atmospheric oxidant is hydroxyl radical (OH) which transforms SO_2 to H_2SO_4. Then, H_2SO_4 is neutralized by NH_3 forming $(NH_4)_2SO_4$, or dissolves in aerosol liquid water and binds with positive ions like Na^+, leading to the higher shipping-related SO_4^{2-} concentration from the southern Yellow Sea to coastal Fujian in 2017 (Fig. 11a). The maximum of 1.2 μg m^{-3} was located in the waters of Zhoushan Islands. Taking Zhoushan as an example, we found that primary sulfate emitted by ships played a minor role and secondary sulfate accounted for 91.8% of the shipping-related sulfate. As EC is a stable species, the primary sulfate concentration from shipping can be calculated through multiplying the EC concentration from shipping by the ratio of SO_4^{2-} to EC in ship-emitted PM in Table S3. Thus, the secondary part of shipping-related sulfate equals the difference of the total concentration and the primary part. Although the SO_2 concentration from shipping was also at a relatively high level along the Yangtze River, the shipping-related SO_4^{2-} concentration was significantly~~

~~lower compared to the values in sea areas, which was attributed to the competitive mechanism by land-based emissions. In 2021, the shipping related SO_4^{2-} concentration decreased with the reduction in SO_2 emissions, with the maximum of 0.46 μg m^{-3}. There were unexpected negative values over land areas, which was likely due to the depletion of oxidants to generate nitric acid (HNO_3) in areas characterized by high NO_x conditions.~~

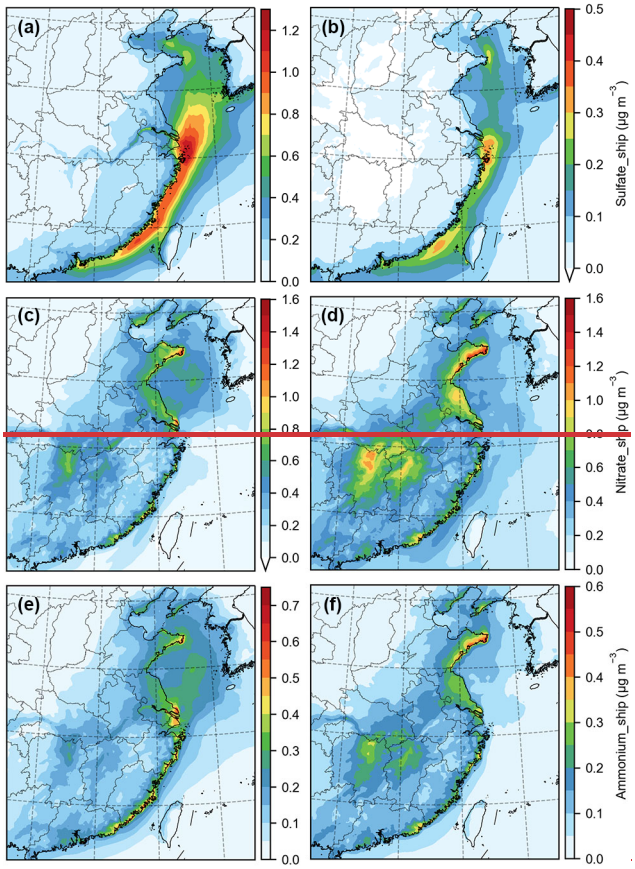

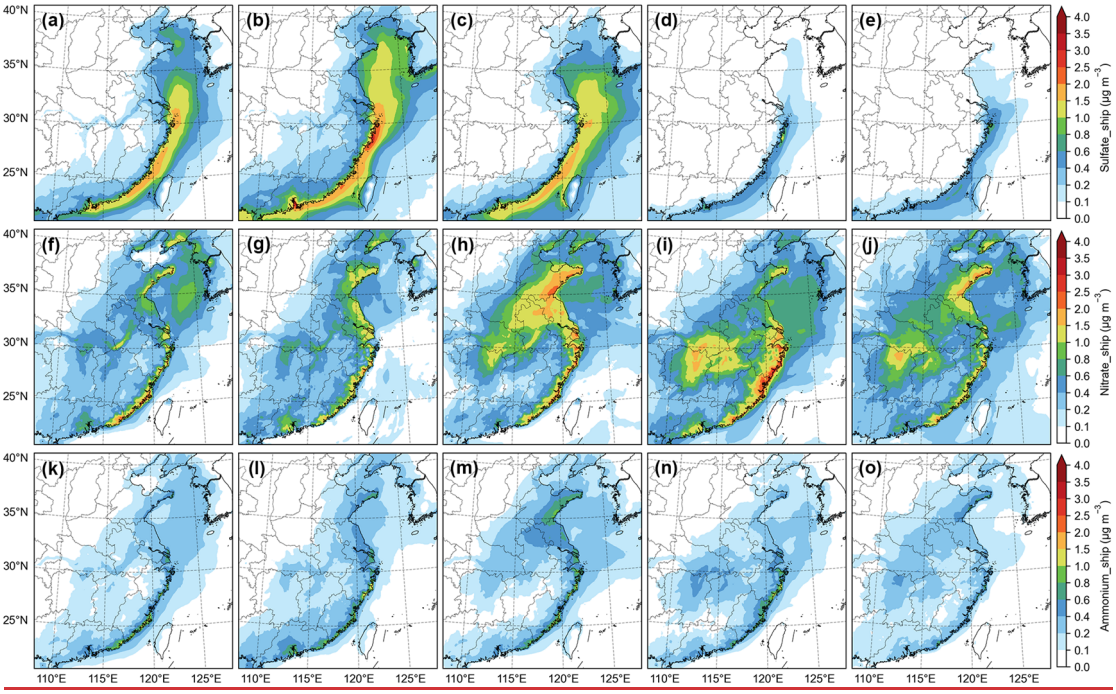

Figure ~~11~~8. Potential impacts of ship emissions on **(a–e)** the sulfate concentrations (Sulfate_ship), **(f–j)** the nitrate ~~(Nitrate_ship)~~ concentrations (Nitrate_ship), and **(k–o)** the ammonium concentrations (Ammonium_ship) in April from 2017 to 2021 in the chronological order from left to right.~~: for sulfate in **(a)** 2017 and **(b)** 2021; for nitrate in **(c)** 2017 and **(d)** 2021; and for ammonium in **(e)** 2017 and **(f)** 2021.~~

Most of initially emitted NO_x is in the form of NO, and is rapidly oxidized to NO_2. During the daytime, NO_2 can be converted to HNO_3 by reacting with OH radicals. During the nighttime, NO_2 combines with NO_3 radicals originating from the oxidization of NO_2 by O_3 to generate dinitrogen pentoxide (N_2O_5). HNO_3 is formed via the reaction of N_2O_5 and water. Compared to HNO_3, NH_3 preferentially reacts with H_2SO_4 because $(NH_4)_2SO_4$ is more stable than NH_4NO_3. Therefore, the formation of particulate nitrate requires sufficient amounts of NH_3. The difference in the formation mechanisms between sulfate and nitrate can explain the significant difference in the spatial patterns of the concentrations between SO_4^{2-} and NO_3^- related to ship emissions. ~~The shipping-related NH_4NO_3 in the marine atmosphere came from NH_3 transported from land areas or the transport of NH_4NO_3 already formed in coastal areas.~~ High SO_4^{2-} ~~I~~concentrations were found in coastal marine areas with plenty radicals, whereas high NO_3^- concentrations generally occurred along the coast with sufficient NH_3 emissions. The P_{99} values of the ~~concentration of~~ shipping-related NO_3^- concentrations showed a similar interannual variation pattern compared to the NO_2 concentrations, with the values of 1.2, 1.1, 1.7, 1.8, and 1.4 μg m^{-3} from 2017 to 2021 year by year. During the DECA 2.0 period, the decrease in the SO_2 emissions provided more opportunities for HNO_3 to be neutralized by NH_3, leading to the noticeable increase in the concentrations

of shipping-related NO_3^- over the land areas of eastern China. In the same way, in the inland emission control areas, the concentrations of shipping-related NO_3^- shipping over the middle reaches of the Yangtze River in 2020 and 2021 under the ultra-low sulfur regulation were remarkably higher than those in 2017 and 2018. ~~only displayed moderate levels over the Yellow Sea in 2017. In comparison, higher concentration levels were concentrated along the coast, with the maximum of 1.4 μg m^{-3} (Fig. 11c). In 2021, the values increased over land areas with the increase in NO_x emissions and the decrease in SO_2 emissions from shipping, while the maximum slightly increased to 1.5 μg m^{-3} located along the coast of Shandong (Fig .11d). There was a noticeable increase in the central Yangtze River Basin, corresponding to the negative values of shipping related SO_4^{2-}.~~ In this study, there was no markedly negative value of shipping-related NO_3^- in the model domain, which differed from the result in the Mediterranean Sea also based on the CMAQ model (Fink et al., 2023a). This was caused by the huge amounts of NH_3 emissions from agriculture in China, providing an ammonia-rich condition to generate NH_4NO_3 (Fig. S11).

The spatial patterns of shipping-related NH_4^+ were similar with those of shipping-related NO_3^- because NH_3 is essential to the formation of particulate nitrate ~~both in 2017 and 2021 (Fig. 11e and Fig. 11f). This result~~. This result also impl~~i~~ied~~ed~~ that the relatively high levels of shipping-related SO_4^{2-} in ammonia-poor offshore areas tended to present in the form of metal salt like Na_2SO_4 rather than $(NH_4)_2SO_4$. Compared to SO_4^{2-} and NO_3^-, the concentration of shipping-related NH_4^+ was at a lower level due to the much smaller molar mass~~,~~. The P_{99} values varied little from year to year, with the values of 0.6, 0.7, 0.7, 0.6, and 0.5 μg m^{-3} from 2017 to 2021, which was due to the balance between the decrease in the sulfate concentrations and the increase in the nitrate concentrations.~~maxima of 0.73 μg m^{-3} in 2017 and 0.58 μg m^{-3} in 2021. Overall, higher levels of potential impacts of ship emissions on SO_4^{2-} occurred in marine areas, while in land areas for NO_3^- and NH_4^+. Given that $PM_{2.5}$ especially secondary species like nitrate was underestimated in China's coastal cities in this study as discussed in Sect. 3.2, the simulated concentrations of SNA related to ship emissions were conservative.~~

3.4.4 Organic aerosols

Organic aerosol (OA) is categorized into primary organic aerosol (POA) and secondary organic aerosol (SOA). POA is calculated as the sum of particulate organic carbon (POC) and particulate non-carbon organic matter (PNCOM), two species in the AERO7 module. ~~POA and EC share similar atmospheric processes in the CMAQ model.~~ The spatial pattern of the POA concentrations from shipping was similar

with that of the SO_2 concentrations from shipping. The P_{99} values in the spring of 2017−2021 were 0.3, 0.4, 0.3, 0.1, and 0.1 μg m^{-3} in the chronological order. The P_{99} value was reduced by 34.7% and further by 57.4% due to the staged policy shifts. In this study, the sum of the contributions of POC and PNCOM to primary $PM_{2.5}$ emitted by ships using HSFO was set to 70.8%, while this value was reduced to 33.4% in the case of burning LSFO (Table ~~S3~~S4). Thus, the reduction in the POA concentrations from shipping due to the fuel type change was more significant ~~than those in the primary $PM_{2.5}$ concentration from shipping and also~~compared to the total shipping-related $PM_{2.5}$ concentrations. ~~The maximum value decreased from 0.41 μg m^{-3} in 2017 to 0.12 μg m^{-3} in 2021 (Fig. S7). The contribution of ship emissions to the ambient POA concentration showed higher values compare to the $PM_{2.5}$ concentration share, with the maximum of 41.9% in 2017 and 29.4% in 2021. The transport of secondary aerosols related to land-based emissions as well as the restricted secondary aerosol formation in marine areas with the NH_3 poor conditions led to lower values of the $PM_{2.5}$ concentration share.~~

SOA, a kind of photochemical product, is produced via the reactions of VOCs or semi-volatile organic compounds (SVOCs) with atmospheric oxidants. ~~As discussed in Sect. 3.2, this study showed the potential impacts of ship emissions on atmospheric photochemistry by using the zero-out method, which differed from the situations of the real-world atmosphere such as the chemical processes in a single ship plume.~~ The P_{99} values of the shipping-related SOA concentrations from 2017 to 2021 were 1.6, 1.9, 1.3, 0.5, and 0.5 μg m^{-3} year by year and were 4−5 times as much as those of the POA concentrations from shipping. The P_{99} value was reduced by 29.6% and further by 60.8% due to the staged policy shifts, which was comparable to the pattern of the POA concentrations from shipping.~~The potential impacts of ship emissions on the SOA and SO_4^{2-} concentrations shared similar spatial patterns in 2017, with the maximum of 1.3 μg m^{-3} over the waters of Zhoushan Islands (Fig. 12a). No negative value was found in the entire model domain. However, in 2021, the marine and coastal areas displayed positive values with the maximum of 0.33 μg m^{-3} near the eastern coast of the Pearl River Delta, whereas negative values were obtained in the central Yangtze River Basin with the minimum of −0.33 μg m^{-3} (Fig. 12b).~~

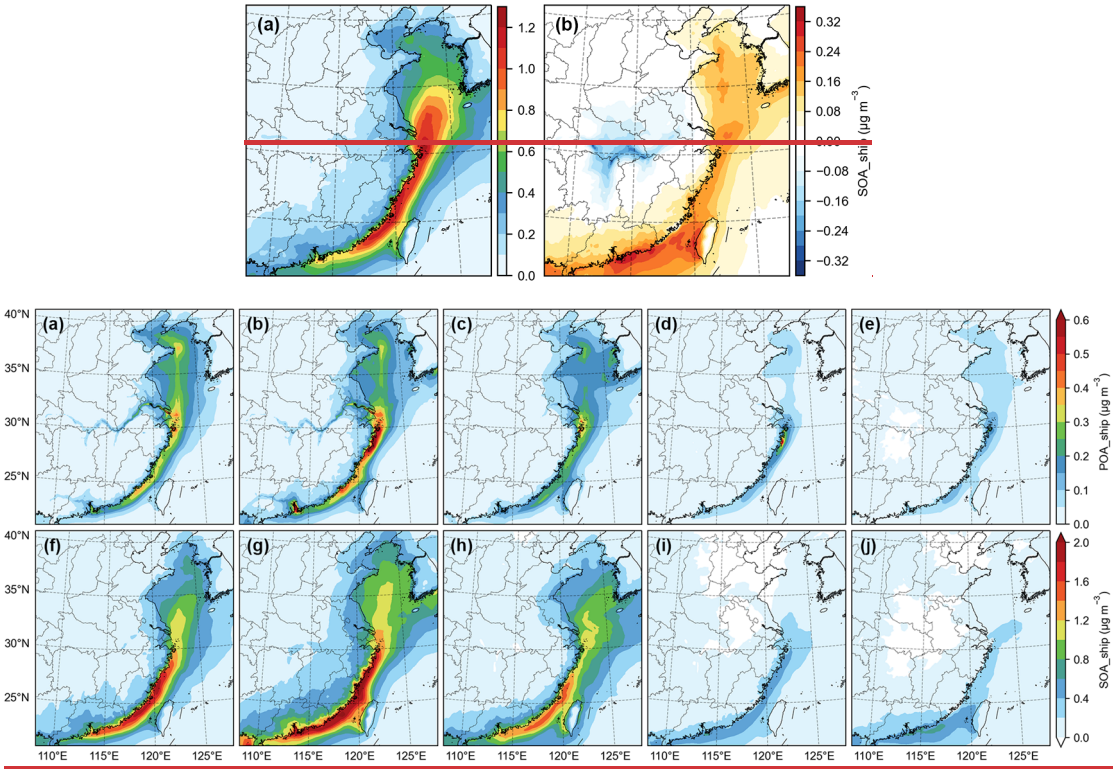

Figure ~~12~~9. Potential impacts of ship emissions on the concentrations of **(a–e)** primary organic aerosols (POA_ship) and **(f–j)** secondary organic aerosols (SOA_ship) in April from 2017 to 2021 in the chronological order from left to right.

~~in **(a)** 2017 and **(b)** 2021.~~

~~For~~The summertime hotspots of the shipping-related $PM_{2.5}$ concentrations were corresponding to the high SOA concentrations in the eastern offshore areas (~~, the seasonal patterns of the shipping-related SOA concentration shown in~~ Fig. ~~S8~~S12)~~., the highest level in the eastern offshore areas of China was found in the summer of both 2017 and 2021.~~ In summer, high temperature and good lighting conditions are in favor of BVOC emissions and photochemical reactions, resulting in abundant oxidants in the background atmosphere to generate O_3, sulfate, and SOA. Ship emissions could increase the concentrations of O_3 and SOA in the NO_x-limited marine atmosphere with low NO_x concentrations. Although the NO_x and VOCs emissions from shipping increased from 2017 to 2021, the shipping-related SOA concentrations ~~during the summertime~~in summer decreased. This result suggested that the decrease in the shipping-related PM was likely to reduce the impact of gas-particle partitioning ~~This result suggested that gas-particle partitioning~~ of organic matter with low to medium volatility ~~played an important role in SOA formation~~. ~~The significant decrease in the shipping-related PM was likely to reduce the impact of gas-particle partitioning. In contrast to the pattern in summer, t~~The potential impact of ship emissions on SOA showed

negative values in inland areas in the winter of 2021, which was indirectly caused by the O_3 titration by NO_x under the VOC-limited regime. ~~The potential impact was insignificant in the other seasons, and thus the annual mean values in central China were negative. The increasing NO_x emissions along the Yangtze River led to more depletion in oxidants over inland areas during the wintertime. The minimum shipping-related SOA concentration in winter decreased from -0.45 μg m^{-3} in 2017 to -1.0 μg m^{-3} in 2021.~~

3.5 Intercomparison of the impacts over the port cities

In Sect. 3.5, the perspective will be shifted from a regional scale to an urban scale. For each of the 21 port cities selected in this study, the data of the grids where populous downtown areas (instead of the ports themselves) are located was extracted for the analysis on the impacts of ship emissions. Thus, the results can reflect the role of ship emissions in the presence of large amounts of land-based emissions in urban areas.

3.5.1 Effects of the IMO Regulation

Figure 1~~0~~3 shows the absolute and relative impacts of ship emissions on multiple species such as SO_2, NO_2, $PM_{2.5}$, SO_4^{2-}, NO_3^-, NH_4^+, carbonaceous aerosol (CA, referred to the sum of OA and EC), V, and Ni at the annual average level in China's main port cities in 2017 and 2021. On average across all the concerned cities with the 95% confidence intervals (CIs), the SO_2 concentration from shipping was reduced from 1.3±0.4 μg m^{-3} in 2017 to 0.48±0.12 μg m^{-3} in 2021 due to ~~the implementation of~~ the IMO Regulation. Its reduction rate was 63.3%, closed to the reduction rate of SO_2 emissions from shipping in the CECA and inland areas of China (68.4%). The share of the SO_2 concentration from shipping was (14.3±5.5)% in 2017 and decreased to (9.0±4.0)% in 2021. However, the NO_2 concentration from shipping increased from 4.3±1.1 μg m^{-3} to 7.1±5.6 μg m^{-3} due to the growth in shipping activities. The increase rate (65.9%) was higher than that of the NO_x emissions from shipping (51.8%), because ship emissions increased the atmospheric oxidation capacity in offshore areas and more NO could be oxidized to NO_2. The share of the NO_2 concentration from shipping rose from (13.9±5.6)% to (22.6±6.2)%.

The shipping-related $PM_{2.5}$ concentration was reduced from 1.6±0.2 μg m^{-3} to 1.1±0.1 μg m^{-3}, and the reduction rate (32.7%) was very closed to that of the $PM_{2.5}$ emissions from shipping (32.8%). The shipping-related $PM_{2.5}$ concentrations in the city level ranged from 0.8~~4~~ μg m^{-3} in ~~Qinzhou~~ QZ to 2.7 μg m^{-3} in ~~Zhoushan~~ ZS in 2017, while from 0.6~~3~~ μg m^{-3} in ~~Yingkou~~ YK to 1.6 μg m^{-3} in ~~Qingdao~~ QD in

2021. It is noted that only ~~Qinzhou~~ QZ experienced an increase, though very small, ~~(0.04 μg m^{-3}),~~ which was corresponding to the intense growth in cargo throughput of the Beibu Gulf ports approaching 100% in the past six years. After the operation of the Pinglu Canal at the end of 2026, there is still great potential for the ~~growth~~ increase in the impacts of ship~~ping activitie~~ emissions on air quality in this area. ~~and thus the impacts of ship emissions on the air quality in Qinzhou will be much more significant if the current policies do not change.~~ Compared to SO_2 and NO_2, the contribution of ship emissions to the total $PM_{2.5}$ concentration only showed a slight change from (6.8±1.6)% to (5.5±1.0)%. The shipping-related $PM_{2.5}$ shares in the city level ranged from 3.0% in ~~Yingkou~~ YK to 17.4% in ~~Zhoushan~~ ZS in 2017, while from 2.5% in ~~Nanjing~~ NJ to 10.3% in ~~Zhoushan~~ ZS in 2021. Unexpectedly, they showed slight increases in five cities adjacent to the Yellow Sea including ~~Dalian~~DL, Y~~antai~~T, Q~~ingda~~D~~o~~, R~~izhao~~Z, and LYG~~ianyungang~~, which was in accord with the increase in the shipping-related NO_3^- and NH_4^+ concentration shares.

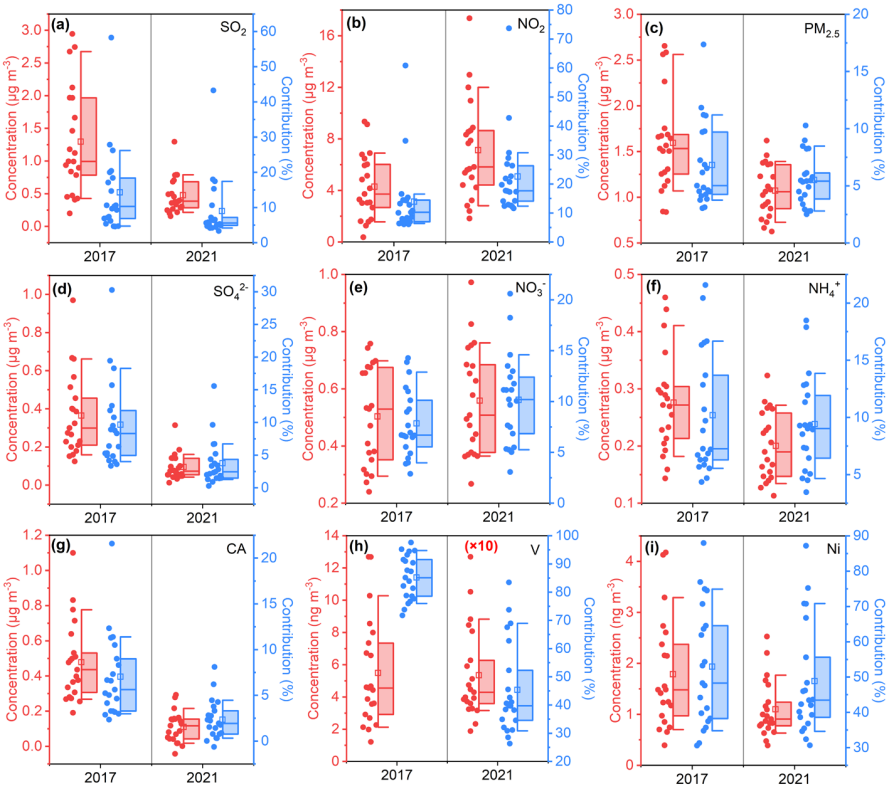

Figure ~~13~~10. Impacts of ship emissions on **(a)** SO_2, **(b)** NO_2, **(c)** $PM_{2.5}$, **(d)** SO_4^{2-}, **(e)** NO_3^-, **(f)** NH_4^+, **(g)** carbonaceous aerosol (CA), **(h)** V, and **(i)** Ni over the representative port cities of China in 2017 and 2021. The concentration boxes are colored in red corresponding to the left axes, while the contribution boxes are colored in blue corresponding to the right axes. ~~Left axis and right axis show concentration and contribution, respectively.~~ Box plots show the mean (square), median (-), lower and upper quartile (boxes), and the 10th and the 90th percentiles (whiskers) of the simulated results. The V concentrations in 2021 ~~is~~ are multiplied by 10.

For the chemical species in the shipping-related $PM_{2.5}$, the SO_4^{2-} concentration was reduced from 0.364±0.1 μg m^{-3} to 0.109±0.0 μg m^{-3}, with the reduction rate of 74.0%, higher than that of the SO_2 concentration from shipping. In contrast, the shipping-related NO_3^- concentration increased by 11.0% from 0.50±0.0 μg m^{-3} to 0.656±0.1 μg m^{-3}. Nevertheless, its increase rate was much smaller than that of the NO_2 concentration from shipping, indicating a low nitrogen oxidation rate (NOR). The weakened sulfate formation was demonstrated by the decrease in the contribution of the secondary SO_4^{2-} to the total SO_4^{2-} related to shipping from (90.0±2.0)89.8% to (77.783.9±10.0)%. Because the decrease in SO_4^{2-} was more significant than the increase in NO_3^-, the shipping-related NH_4^+ concentration decreased by 27.58.6% from 0.328±0.0 μg m^{-3} to 0.20±0.0 μg m^{-3}. The shipping-related CA concentration decreased from 0.485±0.1 μg m^{-3} to 0.11±0.0 μg m^{-3}, with a reduction rate of 76.9%, even higher than that of SO_4^{2-}. The V concentration from shipping sharply dropped from 5.5±1.5 ng m^{-3} to 0.53±0.1 ng m^{-3}. In comparison, the Ni concentration from shipping decreased moderately from 1.8±0.5 ng m^{-3} to 1.1±0.2 ng m^{-3}. The reduction rates of the V and Ni concentrations from shipping were 90.3% and 38.4% respectively, closed to the reduction rates of the emissions of V (90.8%) and Ni (42.0%) from shipping. In addition, the relative impacts of ship emissions on the concentrations of SO_4^{2-}, NO_3^-, NH_4^+, CA, V, and Ni were (9.6±3.0)%, (7.9±1.5)%, (10.2±2.4)%, (7.0±2.0)%, (85.2±3.5)%, and (52.9±7.6)% in 2017 and, while (3.8±1.6)%, (10.2±2.0)%, (9.4±1.8)%, (2.4±0.9)%, (45.4±7.3)%, and (48.9±7.1)% in 2021, respectively. Among the six species, only NO_3^- exhibited an increasing trend in the relative impact.

Figure 114 presents the simulated chemical speciation of $PM_{2.5}$ from all sectors and shipping over China's main port cities in 2017 and 2021. Six categories of chemical species contributing more than 95% to $PM_{2.5}$ were considered which include SO_4^{2-}, NO_3^-, NH_4^+, POA, SOA, and Soil. Soil, a variable in the CMAQ model output, is calculated following Eq. (1):

$$Soil = 2.20 \times Al + 3.48 \times Si + 1.63 \times Ca + 2.42 \times Fe + 1.94 \times Ti \quad (1)$$

The change in the characteristics of the shipping related $PM_{2.5}$ components was far more significant compared to the $PM_{2.5}$ derived by the base runs. SO_4^{2-} accounted for (21.02±2.8)% in the shipping-related $PM_{2.5}$ averaged for the concerned port cities in 2017 and decreased to (8.99.3±2.4)% in 2021, while the percentage of SO_4^{2-} in the $PM_{2.5}$ from all sectors only decreased from (16.716.1±1.3)% to (14.75.0±0.9)%. This result is regarded as the potential impact and does not suggest that ship-emitted $PM_{2.5}$ contains less sulfate content than $PM_{2.5}$ from land-based sources. The SO_4^{2-} shares displayed lower values in the northern region and higher values in the southern region, which may be partly related to the lower aerosol

acidity in the northern region (Wang et al., 2022). ~~Zhoushan, with low NH_3 emissions, showed the highest SO_4^{2-} shares both in 2017 (33.9%) and 2021 (23.2%).~~

In the low-sulfur era, ship emissions tend to enhance the nitrate formation in the high-HNO_3 and high-NH_3 but low-H_2SO_4 conditions in China's coastal cities. Accordingly, NO_3^- has become the major component of the shipping-related $PM_{2.5}$, with the average NO_3^- share increasing from (3~~0.7~~2.2±4.8)% to (54.~~6~~7±5.0)%. The NH_4^+ share also showed an increasing trend from (17.0±0.8)% to (19.6±1.3)% as the decrease in the SO_4^{2-} share cannot offset the increase in the NO_3^- share. In comparison, in the $PM_{2.5}$ from all sectors, the NO_3^- share slightly increased from (~~29.5~~28.1±2.6)% to (30.5~~1.6~~±2.5)%, while the NH_4^+ share changed little from (12.~~5~~2±0.6)% to (1~~2.1~~1.8±0.8)%. The sum of SNA share in the shipping-related $PM_{2.5}$ rose from (70.4~~69.7~~±2.8)% to (83.~~5~~6±4.2)%, whereas that in the $PM_{2.5}$ from all sectors remained at the same level of ~~~~58~~57%. The $PM_{2.5}$ pollution from shipping which coastal urban areas suffer is mainly caused by the transport and aging processes of pollutants emitted by ships in the atmosphere from water to land, which can explain the higher SNA share in the shipping-related $PM_{2.5}$.~~–~~

~~However,~~For the organic aerosols, there contribution to shipping-related $PM_{2.5}$ ~~share~~ decreased from (28.~~4~~5±2.7)% to (10.6~~9.0~~±3.7)%. The SOA share ~~reduce~~decreased from (21.8~~2.2%~~±2.6)% to (5.~~6~~3±3.6)%, and the decrease in the SOA share was much more significant than that in the POA share. The EC share increased from (0.7~~8~~±0.2)% to (1.8±0.4)%, corresponding to the increase in the mapping factors of particulate EC (PEC) for ship emissions from ~~4~~.1% to 7.0%. Due to the substantial contribution of SNA, the EC shares in the shipping-related $PM_{2.5}$ were significantly lower than those in the primary $PM_{2.5}$ from shipping.

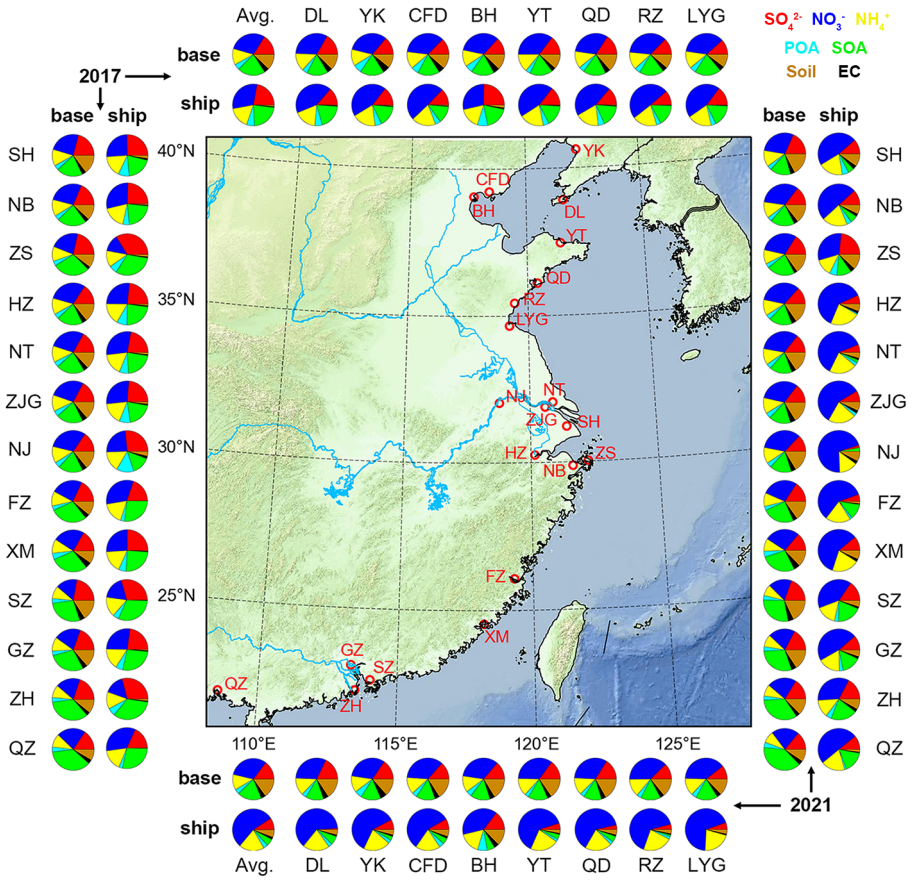

Figure 1411. Simulated chemical speciation of $PM_{2.5}$ from all sectors (base) and shipping (ship) over the representative main port cities of China in 2017 (left and top) and 2021 (right and bottom). Avg. denotes the annual average. DL, YK, CFD, BH, YT, QD, RZ, LYG, SH, NB, ZS, HZ, NT, ZJG, NJ, FZ, XM, SZ, GZ, ZH, and QZ are the abbreviations of Dalian, Yingkou, Caofeidian, Binhai, Yantai, Qingdao, Rizhao, Lianyungang, Shanghai, Ningbo, Zhoushan, Hangzhou, Nantong, Zhangjiagang, Nanjing, Fuzhou, Xiamen, Shenzhen, Guangzhou, Zhuhai, and Qinzhou, respectively. The cities in the northern region are placed at the top and bottom, while the cities in the southern region are placed on the left and right.

~~Regarding the shipping-related PM2.5, the reduction in primary PM2.5 emissions made SNA more important, with the total SNA share rising from 69.7% to 83.4%. However, the organic aerosol share decreased from 28.4% to 9.0%. The SOA share reduced from 22.2% to 5.6%, and the decrease in the SOA share was much more significant than that in the POA share. The EC share increased from 0.8% to 1.8%, corresponding to the increase in the mapping factors of particulate EC (PEC) for ship emissions from 4.1% to 7.0%. Due to the substantial contribution of SNA, the EC shares in the shipping-related PM2.5 were significantly lower than those in the primary PM2.5 from shipping.~~

~~At the city level, both the highest NO3- and NH4+ shares in the shipping-related PM2.5 in 2017 were found in Rizhao corresponding to the lowest SO42- share. However, these values were obtained in Nanjing in the inland ultra-low sulfur control areas, with the NO3- share up to 70.7%. The SO42- shares displayed lower values in the northern region and higher values in the southern region, which may be partly related to the lower aerosol acidity in the northern region (Wang et al., 2022). Zhoushan, with low NH3 emissions, showed the highest SO42- shares both in 2017 (33.9%) and 2021 (23.2%).~~

3.5.2 Roles of the meteorological factors

Meteorological factors can affect both physical and chemical processes of atmospheric pollutants. Considering the complexity of non-linear chemistry discussed above, we focused on the physical aspects here to clarify the roles of meteorological factors on the spatiotemporal patterns of primary PM from shipping in the concerned port cities. We utilized V as the tracer since V is the most convincing tracer of ship emissions and does not participate any chemical process in the model. The impact of temporal variations of emissions was removed because the monthly ship emissions were evenly allocated by hour in this study. Although this simplification smoothed out the time series of the impacts of ship emissions, it contributed to the discussion on the effects of meteorological factors such as wind patterns and the PBLH. Ship emission inventories will be produced in hourly resolution based on the AIS data and used in monthly to long-term simulations in our future work.

Figure ~~15~~ 12 delineates the diurnal variations of the V concentration from shipping over the port cities in every season of 2017 when ship emissions dominated the sources of ambient V. The lowest values

occurred at noon in most cases, corresponding to the highest PBLH. However, the time when the highest values appeared showed significant differences by city, even by season in the same city. If the PBLH plays a crucial role, the V concentration will simply increase with the reduction of the PBLH and reach the peak level in early morning. This pattern was found in four cities in the YRD including ~~Shanghai~~SH, ~~Hangzhou~~HZ, ~~Nantong~~NT, and ~~Zhangjiagang~~ ZJG in every season. A secondary peak during 20:00–21:00 was observed in ~~Shanghai~~ SH in summer, though subtle, which was caused by the intrusion of the sea breeze after the dissipation of the daytime weak convergence (Shang et al., 2019; Zhai et al., 2023). ~~Shanghai~~ SH is more likely to be affected by large synoptic systems, and urbanization results in a weaker land-breeze pattern; meanwhile, the contribution of inland ship emissions is considerable in downtown ~~Shanghai~~SH. The simulation results confirmed the finding in our previous study conducted in ~~Shanghai~~ SH based on field observation (Yu et al., 2021).

In ~~Zhuhai~~ZH, S~~henzhen~~Z, and F~~uzhou~~Z, the V concentrations from shipping peaked before midnight with values significantly higher than those during early morning in every season, indicating that the sea-land breeze circulation (SLBC) significantly affected the diurnal patterns in these cities, especially ~~Zhuhai~~ZH. The SLBC impact in downtown ~~Guangzhou~~ GZ was much weaker than that in ~~Zhuhai~~ ZH and ~~Shenzhen~~SZ, which was due to the dense inland shipping activities in ~~Guangzhou~~GZ. In ~~Binhai~~BH, ~~Caofeidian~~CFD, and ~~Yingkou~~YK, three ports located in the Bohai Bay, the SLBC impact was significant in at least three seasons. In comparison, the SLBC impact ~~on the diurnal variations~~ was smaller in QD~~ingdao~~ and ~~Rizhao~~RZ, two cities adjacent to the Yellow Sea. Nevertheless, this impact was found in every season; the land-breeze could block the transport of ship emissions from marine areas and counteract the PBL compression effect. In ~~Dalian~~ DL and Y~~anta~~T~~i~~, the SLBC impact was noticeable in summer and autumn. The SLBC impact was found in a certain season such as summer in ~~Ningbo~~ NB and ~~Zhoushan~~ ZS while winter in ~~Xiamen~~XM. This study adopted the grid resolution of 9 km and still characterized the ~~impact of the~~ SLBC, a type of ~~local~~ local-scale system. The results in this study are rather different from those in a study conducted in the eastern United States with scarce SLBC impacts using the WRF-CAMx (Golbazi and Archer, 2023).

Besides, the seasonal variations of the V concentrations from shipping in the port cities are also shown in Fig. ~~15~~12. The concentration peaked in spring in most of the cities due to the weak onshore airflows. ~~Shanghai~~SH, ~~Zhoushan~~ZS, N~~antong~~T, ~~Fuzhou~~FZ, and ~~Xiamen~~XM, located along the eastern to southeastern coast exhibited the lowest levels in autumn. The lowest levels were observed in winter for

all the northern cities affected by the prevailing northwesterly wind as well as two southern cities (~~Guangzhou~~ GZ and ~~Shenzhen~~ SZ) affected by the prevailing northeasterly wind. The winter monsoon was adverse to the transport of ship emissions to these cities. In the other cities, poor diffusion conditions enhanced the wintertime concentration levels. It is of interest that cities close in distance did not always perform the same seasonal pattern. For example, in the YRD, ~~Ningbo~~ NB and Z~~houshan~~S, adjacent to each other, showed different seasonal patterns. The southerly wind in July was conducive to the transport of pollutants emitted by ships in N~~ingbo Port~~B to the Z~~houshan Islands~~S, whereas the northerly wind in January and the northeasterly wind in October had an opposite effect~~s~~. ~~In the PRD, Guangzhou and Shenzhen were right located downwind of dense ship emissions in July when the southerly to southeasterly airflows prevailed, and thus the V concentration from shipping was at a relatively high level. However, for Zhuhai, located in the southwest of the PRE, the increase in the V concentration caused by ship emissions was the smallest in summer. Therefore, i~~In addition to the airflow intensity, the relationship between areas with high ship emissions and prevailing airflow directions is an important factor affecting the seasonal pattern of the concentrations of primary PM emitted by ships in receptor cities. Combined with the result that secondary aerosols dominate the $PM_{2.5}$ concentrations from shipping, our findings suggest that it is important to consider both transport pathways and secondary aerosol formation mechanisms to combat the $PM_{2.5}$ pollution caused by shipping in different regions.

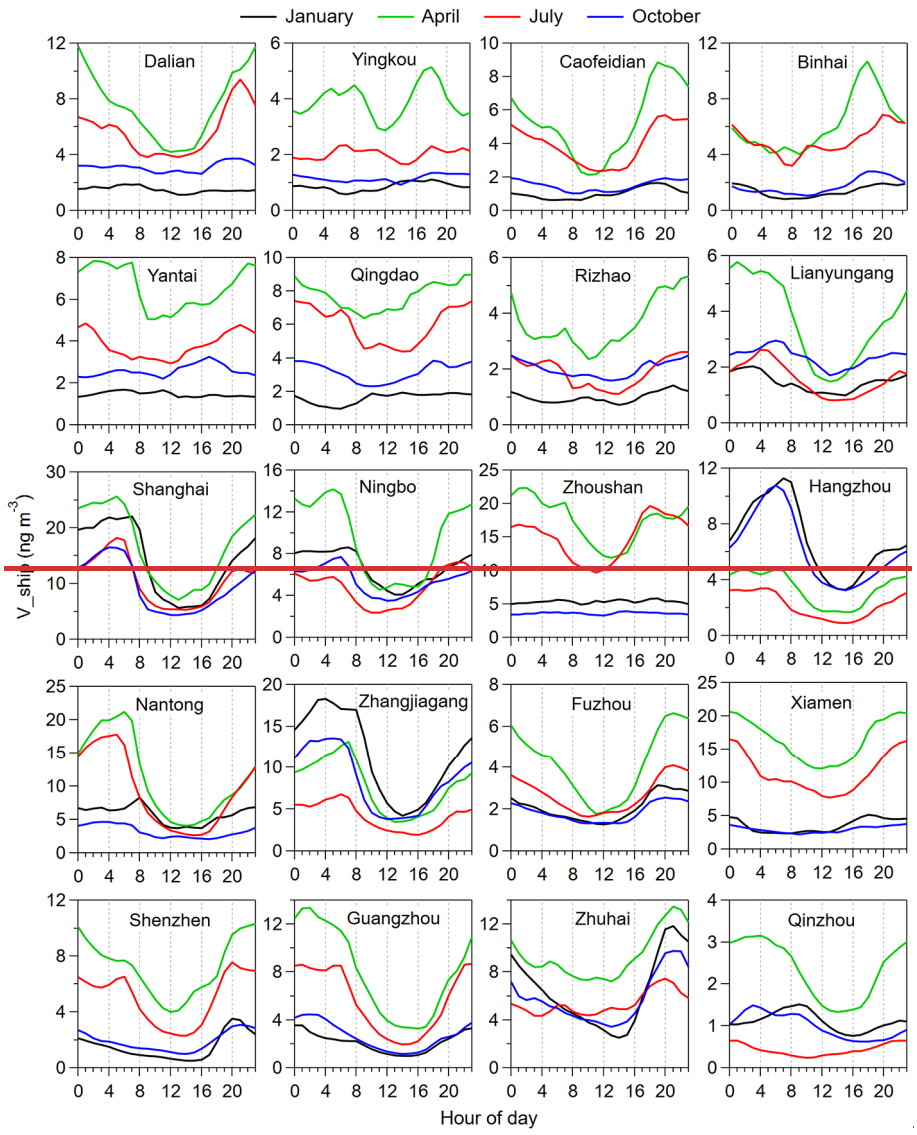
January
April
July
October
Dalian
Yingkou
Caofeidian
Binhai
Yantai
Qingdao
Rizhao
Lianyungang
Shanghai
Ningbo
Zhoushan
Hangzhou
Nantong
Zhangjiagang
Fuzhou
Xiamen
Shenzhen
Guangzhou
Zhuhai
Qinzhou
V_shi (ng m-3)
Hour of day

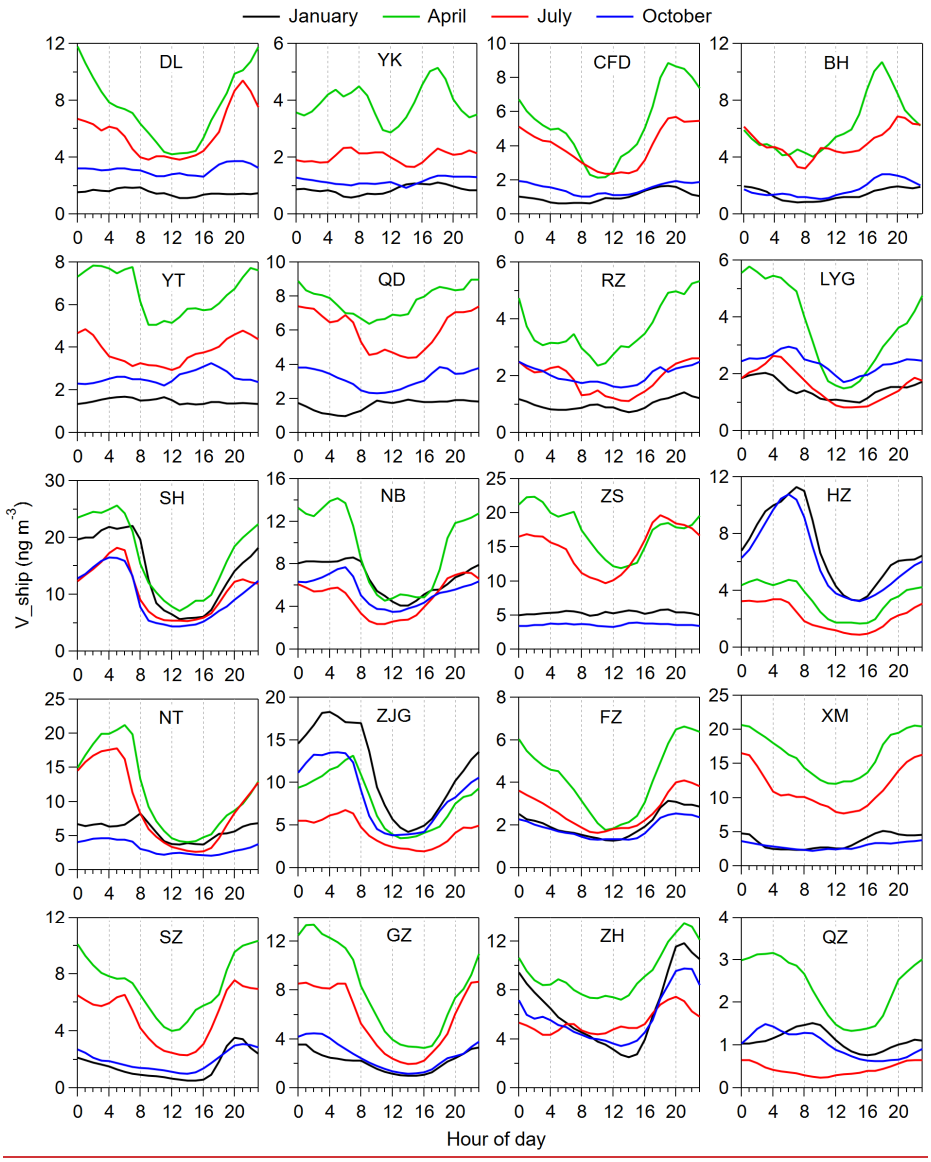

Figure ~~15~~12. Simulated diurnal variations of the V concentrations from shipping (V_ship) over the representative port cities of China in January, April, July, and October of 2017.

4 Conclusions

To meet the requirements of the IMO Regulation, China carried out staged fuel oil policies for sea-going vessels including the DECA 1.0 and the DECA 2.0 which took into effect in 2017 and 2019, respectively. Besides, the inland emission control areas were implemented in 2019 and became more stringent in 2020. It is of significance to evaluate the effects of the staged ~~low sulfur fuel~~ policies on air quality in China ~~in the context of increasing shipping activities~~. We updated the ship emission inventory in China to 2021 based on the AIS data. The emissions of V and Ni from shipping were constrained by the field observational data and the results of on-board emission measurements. The WRF/CMAQ model

were utilized to simulated the impacts on $PM_{2.5}$ in China as well as its gas precursors (SO_2 and NO_2) and components from 2017 to 2021 based on the zero-out method. ~~The model reproduced the V and Ni concentrations as well as their seasonal and diurnal variations, whereas underestimated the secondary aerosol concentrations.~~

In the CECA and inland areas of China, the SO_2, $PM_{2.5}$, V and Ni emissions from shipping were reduced by 68.4%, 32.8%, 90.8%, and 42.0% respectively from 2017 to 2021 due to the IMO Regulation and China's inland river emission control areas. However, the NO_x emissions from shipping increased by 51.8% ~~on monthly averages were 40.9 kt, 7.6 kt, 118.8 t, 41.6 t in 2017, and dropped to 12.9 kt, 5.1 kt, 11.0 t, and 24.1 t in 2021, respectively. The NO_x emissions from shipping increased by 51.8% from 2017 to 2021~~ due to the increase in shipping activities. ~~However, the emissions of SO_2, $PM_{2.5}$, V, and Ni from shipping reduced by 68.4%, 32.8%, 90.8%, and 42.0%, respectively, due to the implementation of the IMO Regulation and China's inland river emission control areas.~~

At the domain level, due to the policy shift from the DECA 1.0 to the DECA 2.0, the P_{99} values of the concentrations of SO_2, $PM_{2.5}$, V, Ni, SO_4^{2-}, POA, and SOA contributed by shipping were reduced by 49.7%, 19.5%, 44.1%, 33.3%, 15.8%, 34.7%, and 29.6%, respectively. The reduction rate of $PM_{2.5}$ was significantly lower than that of SO_2, which was attributed to the increase in NH_4NO_3 along the coast and the transport of aged aerosols with high-sulfur content from the marine areas outside the CECA. Due to the policy shift from the DECA 2.0 to the IMO Regulation, they further decreased by 53.8%, 35.6%, 84.5%, 21.6%, 66.1%, 57.4%, and 60.8%, respectively. However, the impacts of the staged policy shifts on the P_{99} values of the NO_2 concentrations from shipping were within ±5%. Regarding the annual average, ship emissions increased the $PM_{2.5}$ concentrations up to 3.8 μg m^{-3} in 2017 and 2.6 μg m^{-3} in 2021 along China's coastal areas. ~~The SO_2 and NO_2 concentrations from shipping showed higher values along the main routes and spread to both sides. The maximum SO_2 (NO_2) concentrations from shipping were 6.1 μg m^{-3} (17.9 μg m^{-3}) in 2017 and 2.5 μg m^{-3} (26.0 μg m^{-3}) in 2021. In most areas, the peak values occurred in spring while autumn for the valley values, which was attributed to the direction and intensity of the prevailing airflows. The shipping related $PM_{2.5}$ concentration displayed more uniform spatial patterns. In 2017, the areas with concentrations over 1 μg m^{-3} covered most of the Yellow and Bohai Seas and extended to the Middle Yangtze River, with the maximum of 3.8 μg m^{-3} near Zhoushan Islands. In 2021, these areas shrunk to the coast and the central Yangtze River Basin in 2021, with the maximum of 2.6 μg m^{-3} in the eastern Shandong Peninsula.~~ The seasonal pattern~~s~~ of the shipping-related $PM_{2.5}$

concentrations wasdiffered by region mainly due toaffected by the seasonality of secondary aerosol formation, whereas those that of the contributions of ship emissions to the $PM_{2.5}$ concentrations –wasas also affecteddriven by the East Asian Monsoon considering the impacts of land-based sources. The shipping related $PM_{2.5}$ concentration peaked in spring when the SNA formation was significant under the conditions of weak onshore airflows and abundant gas precursors. The offshore marine areas suffered from higher SOA concentration related to ship emissions in summer. The northeasterly airflows diluted the pollution caused by shipping in autumn. NH_3 was consumed by land-based emissions in prior to ship emissions in winter, leading to low shipping related $PM_{2.5}$ concentration in winter. The springtime concentrations of shipping related $PM_{2.5}$, V, and Ni experienced staged reduction in most simulated areas from 2018 to 2021.

At the city level, the contributions of ship emissions to the $PM_{2.5}$ concentration over China's main port cities ranged from 3.0% to 17.4% in 2017 and 2.5% to 10.3% in 2021. The change rates of the concentrations of $PM_{2.5}$, SO_4^{2-}, NO_3^-, NH_4^+, carbonaceous aerosols, V, and Ni related to ship emissions were -32.7%, -74.0%, +11.0%, -27.5%, -76.9%, -90.3%, and -38.4%, respectively. NO_3^- has become the dominant species accounting for 54.6% in the shipping-related $PM_{2.5}$ after 2020, and can contribute to high levels of nocturnal $PM_{2.5}$ concentration. The increasing NO_x emissions from shipping and their potential impacts on $PM_{2.5}$ and O_3 are of concern, which calls for the expansion of the Tier III Regulation in more coastal waters worldwide. Besides, the sea-land breeze circulation played an important role in the diurnal patterns of the concentrations of primary particulate matter from shipping in most seaports, while a minor role was found in Shanghai and Guangzhou with large inland ship emissions. Our findings suggest that it is important to consider both transport pathways and formation mechanisms of secondary aerosol formation mechanisms s to combat the $PM_{2.5}$ pollution caused by shipping in different regions.

Data availability

The data derived from the ship emission model and the WRF/CMAQ model presented in this paper can be obtained from Yan Zhang (yan_zhang@fudan.edu.cn) upon request.

Author contribution

GY: investigation, methodology, software, validation, formal analysis, data curation, visualization,

funding acquisition, and writing – original draft preparation; YZ: conceptualization, investigation, supervision, methodology, validation, project administration, funding acquisition, and writing – review and editing; QW: validation, data curation, and writing – review; ZH: methodology, software, and data curation; SJ: methodology, software, and data curation; FY: data curation, funding acquisition, and writing – review; XY: writing – review and editing; CH: supervision, data curation, and writing – review and editing

Competing interests

The authors declare that they have no conflict of interest.

Acknowledgements

The work was supported by the National Natural Science Foundation of China (No. 42077195), and the Natural Science Foundation of Shanghai Committee of Science and Technology, China (No. 22ZR1407700), and the Science and Technology Innovation Action Plan of Shanghai (No. 24YF2736200).

References

Agrawal, H., Welch, W. A., Miller, J. W., and Cocker, D. R.: Emission Measurements from a Crude Oil Tanker at Sea, Environmental Science & Technology, 42, 7098-7103, https://doi.org/10.1021/es703102y, 2008a.

Agrawal, H., Malloy, Q. G. J., Welch, W. A., Wayne Miller, J., and Cocker, D. R.: In-use gaseous and particulate matter emissions from a modern ocean going container vessel, Atmospheric Environment, 42, 5504-5510, 2008b.

Agrawal, H., Welch, W. A., Henningsen, S., Miller, J. W., and Cocker, D. R.: Emissions from main propulsion engine on container ship at sea, Journal of Geophysical Research, 115, https://doi.org/10.1029/2009jd013346, 2010.

Agrawal, H., Eden, R., Zhang, X., Fine, P. M., Katzenstein, A., Miller, J. W., Ospital, J., Teffera, S., and Cocker, D. R.: Primary Particulate Matter from Ocean-Going Engines in the Southern California Air Basin, Environmental Science & Technology, 43, 5398-5402, https://doi.org/10.1021/es8035016, 2009.

Aksoyoglu, S., Baltensperger, U., and Prévôt, A. S. H.: Contribution of ship emissions to the concentration and deposition of air pollutants in Europe, Atmospheric Chemistry and Physics, 16, 1895-1906, http://doi.org/10.5194/acp-16-1895-2016, 2016.

Anastasopolos, A. T., Sofowote, U. M., Hopke, P. K., Rouleau, M., Shin, T., Dheri, A., Peng, H., Kulka, R., Gibson, M. D., Farah, P. M., and Sundar, N.: Air quality in Canadian port cities after regulation of low-sulphur marine fuel in the North American Emissions Control Area, Science of the Total

Environment, 791, 147949, https://doi.org/10.1016/j.scitotenv.2021.147949, 2021.

Badeke, R., Matthias, V., Karl, M., and Grawe, D.: Effects of vertical ship exhaust plume distributions on urban pollutant concentration – a sensitivity study with MITRAS v2.0 and EPISODE-CityChem v1.4, Geoscientific Model Development, 15, 4077-4103, https://doi.org/10.5194/gmd-15-4077-2022, 2022.

Celo, V., Dabek-Zlotorzynska, E., and McCurdy, M.: Chemical characterization of exhaust emissions from selected canadian marine vessels: the case of trace metals and lanthanoids, Environmental Science & Technology, 49, 5220-5226, https://doi.org/10.1021/acs.est.5b00127, 2015.

Ministry of Transport of the People's Republic of China: Report on China's Shipping Development in 2022 (in Chinese), 2023.

Chosson, F., Paoli, R., and Cuenot, B.: Ship plume dispersion rates in convective boundary layers for chemistry models, Atmospheric Chemistry and Physics, 8, 4841-4853, https://doi.org/10.5194/acp-8-4841-2008, 2008.

Corbin, J. C., Mensah, A. A., Pieber, S. M., Orasche, J., Michalke, B., Zanatta, M., Czech, H., Massabo, D., Buatier de Mongeot, F., Mennucci, C., El Haddad, I., Kumar, N. K., Stengel, B., Huang, Y., Zimmermann, R., Prevot, A. S. H., and Gysel, M.: Trace Metals in Soot and $PM_{2.5}$ from Heavy-Fuel-Oil Combustion in a Marine Engine, Environmental Science & Technology, 52, 6714-6722, https://doi.org/10.1021/acs.est.8b01764, 2018.

Dalsøren, S. B., Eide, M. S., Endresen, Ø., Mjelde, A., Gravir, G., and Isaksen, I. S. A.: Update on emissions and environmental impacts from the international fleet of ships: the contribution from major ship types and ports, Atmospheric Chemistry and Physics, 9, 2171-2194, https://doi.org/10.5194/acp-9-2171-2009, 2009.

Du, Q., Zhao, C., Zhang, M., Dong, X., Chen, Y., Liu, Z., Hu, Z., Zhang, Q., Li, Y., Yuan, R., and Miao, S.: Modeling diurnal variation of surface $PM_{2.5}$ concentrations over East China with WRF-Chem: impacts from boundary-layer mixing and anthropogenic emission, Atmospheric Chemistry and Physics, 20, 2839-2863, https://doi.org/10.5194/acp-20-2839-2020, 2020.

EMSA – European Maritime Safety Agency and EEA – European Environment Agency: European Maritime Transport Environmental Report 2021, https://doi.org/10.2800/3525, 2021.

Eyring, V., Isaksen, I. S. A., Berntsen, T., Collins, W. J., Corbett, J. J., Endresen, O., Grainger, R. G., Moldanova, J., Schlager, H., and Stevenson, D. S.: Transport impacts on atmosphere and climate: Shipping, Atmospheric Environment, 44, 4735-4771, https://doi.org/10.1016/j.atmosenv.2009.04.059, 2010.

Fan, Q., Zhang, Y., Ma, W., Ma, H., Feng, J., Yu, Q., Yang, X., Ng, S. K., Fu, Q., and Chen, L.: Spatial and Seasonal Dynamics of Ship Emissions over the Yangtze River Delta and East China Sea and Their Potential Environmental Influence, Environmental Science & Technology, 50, 1322-1329, https://doi.org/10.1021/acs.est.5b03965, 2016.

Feng, J., Zhang, Y., Li, S., Mao, J., Patton, A. P., Zhou, Y., Ma, W., Liu, C., Kan, H., Huang, C., An, J., Li, L., Shen, Y., Fu, Q., Wang, X., Liu, J., Wang, S., Ding, D., Cheng, J., Ge, W., Zhu, H., and Walker, K.: The influence of spatiality on shipping emissions, air quality and potential human exposure in the Yangtze River Delta/Shanghai, China, Atmospheric Chemistry and Physics, 19, 6167-6183, https://doi.org/10.5194/acp-19-6167-2019, 2019.

Feng, X., Ma, Y., Lin, H., Fu, T. M., Zhang, Y., Wang, X., Zhang, A., Yuan, Y., Han, Z., Mao, J., Wang, D., Zhu, L., Wu, Y., Li, Y., and Yang, X.: Impacts of Ship Emissions on Air Quality in Southern China: Opportunistic Insights from the Abrupt Emission Changes in Early 2020, Environmental Science & Technology, 57, 16999-17010, https://doi.org/10.1021/acs.est.3c04155, 2023.

Fink, L., Karl, M., Matthias, V., Oppo, S., Kranenburg, R., Kuenen, J., Jutterström, S., Moldanova, J., Majamäki, E., and Jalkanen, J.-P.: A multimodel evaluation of the potential impact of shipping on particle species in the Mediterranean Sea, Atmospheric Chemistry and Physics, 23, 10163-10189, https://doi.org/10.5194/acp-23-10163-2023, 2023a.

Fink, L., Karl, M., Matthias, V., Oppo, S., Kranenburg, R., Kuenen, J., Moldanova, J., Jutterström, S., Jalkanen, J.-P., and Majamäki, E.: Potential impact of shipping on air pollution in the Mediterranean region – a multimodel evaluation: comparison of photooxidants NO_2 and O_3, Atmospheric Chemistry and Physics, 23, 1825-1862, https://doi.org/10.5194/acp-23-1825-2023, 2023b.

Fu, X., Chen, D., Wang, X., Li, Y., Lang, J., Zhou, Y., and Guo, X.: The impacts of ship emissions on ozone in eastern China, Science of the Total Environment, 903, 166252, https://doi.org/10.1016/j.scitotenv.2023.166252, 2023.

Golbazi, M. and Archer, C.: Impacts of maritime shipping on air pollution along the US East Coast, Atmospheric Chemistry and Physics, 23, 15057-15075, https://doi.org/10.5194/acp-23-15057-2023, 2023.

He, L., Wang, J., Liu, Y., Zhang, Y., He, C., Yu, Q., and Ma, W.: Selection of onshore sites based on monitoring possibility evaluation of exhausts from individual ships for Yantian Port, China, Atmospheric Environment, 247, https://doi.org/10.1016/j.atmosenv.2021.118187, 2021.

Hersbach, H., Bell, B., Berrisford, P., Biavati, G., Horányi, A., Muñoz Sabater, J., Nicolas, J., Peubey, C., Radu, R., Rozum, I., Schepers, D., Simmons, A., Soci, C., Dee, D., and Thépaut, J.-N.: ERA5 hourly data on single levels from 1940 to present, Copernicus Climate Change Service (C3S) Climate Data Store (CDS) [dataset], https://doi.org/10.24381/cds.adbb2d47 (last access: 23 March 2023), 2023.

Huang, C., Hu, Q., Wang, H., Qiao, L., Jing, S., Wang, H., Zhou, M., Zhu, S., Ma, Y., Lou, S., Li, L., Tao, S., Li, Y., and Lou, D.: Emission factors of particulate and gaseous compounds from a large cargo vessel operated under real-world conditions, Environmental Pollution, 242, 667-674, https://doi.org/10.1016/j.envpol.2018.07.036, 2018a.

Huang, C., Hu, Q., Li, Y., Tian, J., Ma, Y., Zhao, Y., Feng, J., An, J., Qiao, L., Wang, H., Jing, S., Huang, D., Lou, S., Zhou, M., Zhu, S., Tao, S., and Li, L.: Intermediate Volatility Organic Compound Emissions from a Large Cargo Vessel Operated under Real-World Conditions, Environmental Science & Technology, 52, 12934-12942, https://doi.org/10.1021/acs.est.8b04418, 2018b.

IMO – International Maritime Organization: Fourth IMO GHG Study 2020, London, UK, 2021.

Jang, E., Choi, S., Yoo, E., Hyun, S., and An, J.: Impact of shipping emissions regulation on urban aerosol composition changes revealed by receptor and numerical modelling, npj Climate and Atmospheric Science, 6, 52, https://doi.org/10.1038/s41612-023-00364-9, 2023.

Jiang, S., Zhang, Y., Yu, G., Han, Z., Zhao, J., Zhang, T., and Zheng, M.: Source-resolved atmospheric metal emissions, concentrations, and deposition fluxes into the East Asian seas, Atmospheric Chemistry and Physics, 24, 8363-8381, https://doi.org/10.5194/acp-24-8363-2024, 2024.

Jonson, J. E., Gauss, M., Schulz, M., Jalkanen, J.-P., and Fagerli, H.: Effects of global ship emissions on European air pollution levels, Atmospheric Chemistry and Physics, 20, 11399-11422, https://doi.org/10.5194/acp-20-11399-2020, 2020.

Kang, Y., Liu, M., Song, Y., Huang, X., Yao, H., Cai, X., Zhang, H., Kang, L., Liu, X., Yan, X., He, H., Zhang, Q., Shao, M., and Zhu, T.: High-resolution ammonia emissions inventories in China from 1980 to 2012, Atmospheric Chemistry and Physics, 16, 2043-2058, https://doi.org/10.5194/acp-16-2043-2016, 2016.

Karjalainen, P., Teinila, K., Kuittinen, N., Aakko-Saksa, P., Bloss, M., Vesala, H., Pettinen, R., Saarikoski,

S., Jalkanen, J. P., and Timonen, H.: Real-world particle emissions and secondary aerosol formation from a diesel oxidation catalyst and scrubber equipped ship operating with two fuels in a SECA area, Environmental Pollution, 292, 118278, https://doi.org/10.1016/j.envpol.2021.118278, 2022.

Kotchenruther, R. A.: The effects of marine vessel fuel sulfur regulations on ambient $PM_{2.5}$ along the west coast of the U.S, Atmospheric Environment, 103, 121-128, https://doi.org/10.1016/j.atmosenv.2014.12.040, 2015.

Kotchenruther, R. A.: The effects of marine vessel fuel sulfur regulations on ambient $PM_{2.5}$ at coastal and near coastal monitoring sites in the U.S, Atmospheric Environment, 151, 52-61, https://doi.org/10.1016/j.atmosenv.2016.12.012, 2017.

Lack, D. A., Corbett, J. J., Onasch, T., Lerner, B., Massoli, P., Quinn, P. K., Bates, T. S., Covert, D. S., Coffman, D., Sierau, B., Herndon, S., Allan, J., Baynard, T., Lovejoy, E., Ravishankara, A. R., and Williams, E.: Particulate emissions from commercial shipping: Chemical, physical, and optical properties, Journal of Geophysical Research, 114, https://doi.org/10.1029/2008jd011300, 2009.

Lansø, A. S., Winther, M., Jensen, S. S., and Løfstrøm, P.: Impact on air quality from increasing cruise ship activity in Copenhagen port, Environmental Research Communications, 5, https://doi.org/10.1088/2515-7620/acb90c, 2023.

Li, M., Zhang, Q., Kurokawa, J.-i., Woo, J.-H., He, K., Lu, Z., Ohara, T., Song, Y., Streets, D. G., Carmichael, G. R., Cheng, Y., Hong, C., Huo, H., Jiang, X., Kang, S., Liu, F., Su, H., and Zheng, B.: MIX: a mosaic Asian anthropogenic emission inventory under the international collaboration framework of the MICS-Asia and HTAP, Atmospheric Chemistry and Physics, 17, 935-963, https://doi.org/10.5194/acp-17-935-2017, 2017.

Liu, H., Jin, X., Wu, L., Wang, X., Fu, M., Lv, Z., Morawska, L., Huang, F., and He, K.: The impact of marine shipping and its DECA control on air quality in the Pearl River Delta, China, Science of the Total Environment, 625, 1476-1485, https://doi.org/10.1016/j.scitotenv.2018.01.033, 2018a.

Liu, Y., Xing, J., Wang, S., Fu, X., and Zheng, H.: Source-specific speciation profiles of $PM_{2.5}$ for heavy metals and their anthropogenic emissions in China, Environmental Pollution, 239, 544-553, https://doi.org/10.1016/j.envpol.2018.04.047, 2018b.

Liu, Y., Zhang, W., Bai, Z., Yang, W., Zhao, X., Han, B., and Wang, X.: China Source Profile Shared Service (CSPSS): The Chinese $PM_{2.5}$ Database for Source Profiles, Aerosol and Air Quality Research, 17, 1501-1514, https://doi.org/10.4209/aaqr.2016.10.0469, 2017a.

Liu, Z., Lu, X., Feng, J., Fan, Q., Zhang, Y., and Yang, X.: Influence of Ship Emissions on Urban Air Quality: A Comprehensive Study Using Highly Time-Resolved Online Measurements and Numerical Simulation in Shanghai, Environmental Science & Technology, 51, 202-211, https://doi.org/10.1021/acs.est.6b03834, 2017b.

Luo, Z., Lv, Z., Zhao, J., Sun, H., He, T., Yi, W., Zhang, Z., He, K., and Liu, H.: Shipping-related pollution decreased but mortality increased in Chinese port cities, Nature Cities, 1, 295-304, https://doi.org/10.1038/s44284-024-00050-8, 2024.

Lv, Z., Liu, H., Ying, Q., Fu, M., Meng, Z., Wang, Y., Wei, W., Gong, H., and He, K.: Impacts of shipping emissions on $PM_{2.5}$ pollution in China, Atmospheric Chemistry and Physics, 18, 15811-15824, https://doi.org/10.5194/acp-18-15811-2018, 2018.

Ma, M., Gao, Y., Ding, A., Su, H., Liao, H., Wang, S., Wang, X., Zhao, B., Zhang, S., Fu, P., Guenther, A. B., Wang, M., Li, S., Chu, B., Yao, X., and Gao, H.: Development and Assessment of a High-Resolution Biogenic Emission Inventory from Urban Green Spaces in China, Environmental Science & Technology, 56, 175-184, https://doi.org/10.1021/acs.est.1c06170, 2022.

Moldanová, J., Fridell, E., Popovicheva, O., Demirdjian, B., Tishkova, V., Faccinetto, A., and Focsa, C.: Characterisation of particulate matter and gaseous emissions from a large ship diesel engine, Atmospheric Environment, 43, 2632-2641, https://doi.org/10.1016/j.atmosenv.2009.02.008, 2009.

Moldanová, J., Fridell, E., Winnes, H., Holmin-Fridell, S., Boman, J., Jedynska, A., Tishkova, V., Demirdjian, B., Joulie, S., Bladt, H., Ivleva, N. P., and Niessner, R.: Physical and chemical characterisation of PM emissions from two ships operating in European Emission Control Areas, Atmospheric Measurement Techniques, 6, 3577-3596, https://doi.org/10.5194/amt-6-3577-2013, 2013.

~~Seinfeld, J. H. and Pandis, S. N.: Atmospheric chemistry and physics: from air pollution to climate change, 3rd Edition, John Wiley & Sons, 2016.~~

Shang, F., Chen, D., Guo, X., Lang, J., Zhou, Y., Li, Y., and Fu, X.: Impact of Sea Breeze Circulation on the Transport of Ship Emissions in Tangshan Port, China, Atmosphere, 10, https://doi.org/10.3390/atmos10110723, 2019.

Sindelarova, K., Markova, J., Simpson, D., Huszar, P., Karlicky, J., Darras, S., and Granier, C.: Copernicus Atmosphere Monitoring Service Global Biogenic VOC emissions version 3.1 (CAMS-GLOB-BIOv3.1) [dataset], https://permalink.aeris-data.fr/CAMS-GLOB-BIO (last access: 2023/7/27), 2021.

Song, S.-K., Shon, Z.-H., Moon, S.-H., Lee, T.-H., Kim, H.-S., Kang, S.-H., Park, G.-H., and Yoo, E.-C.: Impact of international Maritime Organization 2020 sulfur content regulations on port air quality at international hub port, Journal of Cleaner Production, 347, https://doi.org/10.1016/j.jclepro.2022.131298, 2022.

Spada, N. J., Cheng, X., White, W. H., and Hyslop, N. P.: Decreasing Vanadium Footprint of Bunker Fuel Emissions, Environmental Science & Technology, 52, 11528-11534, https://doi.org/10.1021/acs.est.8b02942, 2018.

Sun, J., Qin, M., Xie, X., Fu, W., Qin, Y., Sheng, L., Li, L., Li, J., Sulaymon, I. D., Jiang, L., Huang, L., Yu, X., and Hu, J.: Seasonal modeling analysis of nitrate formation pathways in Yangtze River Delta region, China, Atmospheric Chemistry and Physics, 22, 12629-12646, https://doi.org/10.5194/acp-22-12629-2022, 2022.

Tang, L., Ramacher, M. O. P., Moldanová, J., Matthias, V., Karl, M., Johansson, L., Jalkanen, J.-P., Yaramenka, K., Aulinger, A., and Gustafsson, M.: The impact of ship emissions on air quality and human health in the Gothenburg area – Part 1: 2012 emissions, Atmospheric Chemistry and Physics, 20, 7509-7530, https://doi.org/10.5194/acp-20-7509-2020, 2020.

Tao, L., Fairley, D., Kleeman, M. J., and Harley, R. A.: Effects of switching to lower sulfur marine fuel oil on air quality in the San Francisco Bay area, Environmental Science & Technology, 47, 10171-10178, https://doi.org/10.1021/es401049x, 2013.

UNCTAD – United Nations Conference on Trade and Developmen: Review of Maritime Transport 2023: Towards a Green and Just Transition, United Nations Publications, ISBN: 978-992-971-002886-002888, 2023.

Viana, M., Hammingh, P., Colette, A., Querol, X., Degraeuwe, B., Vlieger, I. d., and van Aardenne, J.: Impact of maritime transport emissions on coastal air quality in Europe, Atmospheric Environment, 90, 96-105, https://doi.org/10.1016/j.atmosenv.2014.03.046, 2014.

Wang, G., Tao, Y., Chen, J., Liu, C., Qin, X., Li, H., Yun, L., Zhang, M., Zheng, H., Gui, H., Liu, J., Huo, J., Fu, Q., Deng, C., and Huang, K.: Quantitative Decomposition of Influencing Factors to Aerosol pH Variation over the Coasts of the South China Sea, East China Sea, and Bohai Sea, Environmental Science & Technology Letters, 9, 815-821, https://doi.org/10.1021/acs.estlett.2c00527, 2022.

Wang, X., Shen, Y., Lin, Y., Pan, J., Zhang, Y., Louie, P. K. K., Li, M., and Fu, Q.: Atmospheric pollution from ships and its impact on local air quality at a port site in Shanghai, Atmospheric Chemistry and Physics, 19, 6315-6330, https://doi.org/10.5194/acp-19-6315-2019, 2019.

Wang, X., Yi, W., Lv, Z., Deng, F., Zheng, S., Xu, H., Zhao, J., Liu, H., and He, K.: Ship emissions around China under gradually promoted control policies from 2016 to 2019, Atmospheric Chemistry and Physics, 21, 13835-13853, https://doi.org/10.5194/acp-21-13835-2021, 2021.

Wang, X., Liu, H., Zhang, J., Fu, X., Chen, D., Zhang, W., Yi, W., Lv, Z., Zhang, Q., and He, K.: Global shipping emissions from 1970 to 2021: Structural and spatial change driven by trade dynamics, One Earth, https://doi.org/10.1016/j.oneear.2025.101243, 2025.

WHO – World Health Organization: Air Quality Guidelines - Update 2021, WHO Regional Office for Europe, Copenhagen, Denmark, 2021.

Xie, X., Hu, J., Qin, M., Guo, S., Hu, M., Wang, H., Lou, S., Li, J., Sun, J., Li, X., Sheng, L., Zhu, J., Chen, G., Yin, J., Fu, W., Huang, C., and Zhang, Y.: Modeling particulate nitrate in China: Current findings and future directions, Environment International, 166, 107369, https://doi.org/10.1016/j.envint.2022.107369, 2022.

Yang, L., Zhang, Q., Zhang, Y., Lv, Z., Wu, L., and Mao, H.: Real-world emission characteristics of an ocean-going vessel through long sailing measurement, Science of the Total Environment, 810, 152276, https://doi.org/10.1016/j.scitotenv.2021.152276, 2022.

Yi, W., Wang, X., He, T., Liu, H., Luo, Z., Lv, Z., and He, K.: The high-resolution global shipping emission inventory by the Shipping Emission Inventory Model (SEIM), Earth System Science Data, 17, 277-292, https://doi.org/10.5194/essd-17-277-2025, 2025.

Yu, G., Zhang, Y., Yang, F., He, B., Zhang, C., Zou, Z., Yang, X., Li, N., and Chen, J.: Dynamic Ni/V Ratio in the Ship-Emitted Particles Driven by Multiphase Fuel Oil Regulations in Coastal China, Environmental Science & Technology, 55, 15031-15039, https://doi.org/10.1021/acs.est.1c02612, 2021.

Zetterdahl, M., Moldanová, J., Pei, X., Pathak, R. K., and Demirdjian, B.: Impact of the 0.1% fuel sulfur content limit in SECA on particle and gaseous emissions from marine vessels, Atmospheric Environment, 145, 338-345, https://doi.org/10.1016/j.atmosenv.2016.09.022, 2016.

Zhai, J., Yu, G., Zhang, J., Shi, S., Yuan, Y., Jiang, S., Xing, C., Cai, B., Zeng, Y., Wang, Y., Zhang, A., Zhang, Y., Fu, T. M., Zhu, L., Shen, H., Ye, J., Wang, C., Tao, S., Li, M., Zhang, Y., and Yang, X.: Impact of Ship Emissions on Air Quality in the Greater Bay Area in China under the Latest Global Marine Fuel Regulation, Environmental Science & Technology, 57, 12341-12350, https://doi.org/10.1021/acs.est.3c03950, 2023.

Zhang, F., Xiao, B., Liu, Z., Zhang, Y., Tian, C., Li, R., Wu, C., Lei, Y., Zhang, S., Wan, X., Chen, Y., Han, Y., Cui, M., Huang, C., Wang, H., Chen, Y., and Wang, G.: Real-world emission characteristics of VOCs from typical cargo ships and their potential contributions to secondary organic aerosol and O3 under low-sulfur fuel policies, Atmospheric Chemistry and Physics, 24, 8999-9017, https://doi.org/10.5194/acp-24-8999-2024, 2024.

Zhang, X., Zhang, Y., Liu, Y., Zhao, J., Zhou, Y., Wang, X., Yang, X., Zou, Z., Zhang, C., Fu, Q., Xu, J., Gao, W., Li, N., and Chen, J.: Changes in the SO_2 Level and $PM_{2.5}$ Components in Shanghai Driven by Implementing the Ship Emission Control Policy, Environmental Science & Technology, 53, 11580-11587, https://doi.org/10.1021/acs.est.9b03315, 2019a.

Zhang, Y., Deng, F., Man, H., Fu, M., Lv, Z., Xiao, Q., Jin, X., Liu, S., He, K., and Liu, H.: Compliance and port air quality features with respect to ship fuel switching regulation: a field observation campaign, SEISO-Bohai, Atmospheric Chemistry and Physics, 19, 4899-4916, https://doi.org/10.5194/acp-19-

4899-2019, 2019b.

Zhao, J., Zhang, Y., Xu, H., Tao, S., Wang, R., Yu, Q., Chen, Y., Zou, Z., and Ma, W.: Trace Elements From Ocean-Going Vessels in East Asia: Vanadium and Nickel Emissions and Their Impacts on Air Quality, Journal of Geophysical Research: Atmospheres, 126, e2020JD033984, https://doi.org/10.1029/2020jd033984, 2021.

Zhao, M., Zhang, Y., Ma, W., Fu, Q., Yang, X., Li, C., Zhou, B., Yu, Q., and Chen, L.: Characteristics and ship traffic source identification of air pollutants in China's largest port, Atmospheric Environment, 64, 277-286, https://doi.org/10.1016/j.atmosenv.2012.10.007, 2013.

Zheng, B., Zhang, Q., Geng, G., Chen, C., Shi, Q., Cui, M., Lei, Y., and He, K.: Changes in China's anthropogenic emissions and air quality during the COVID-19 pandemic in 2020, Earth System Science Data, 13, 2895-2907, https://doi.org/10.5194/essd-13-2895-2021, 2021.

Zheng, H., Cai, S., Wang, S., Zhao, B., Chang, X., and Hao, J.: Development of a unit-based industrial emission inventory in the Beijing–Tianjin–Hebei region and resulting improvement in air quality modeling, Atmospheric Chemistry and Physics, 19, 3447-3462, https://doi.org/10.5194/acp-19-3447-2019, 2019.